

High-K states in the odd-odd nuclide ^{180}Re

H.M. El-Masri,¹ P.M. Walker,^{1,*} G.D. Dracoulis,² T. Kibédi,² A.P. Byrne,² A.M. Bruce,³
J.N. Orce,³ A. Emmanouilidis,³ D.M. Cullen,⁴ C. Wheldon,⁵ and F.R. Xu⁶

¹*Department of Physics, University of Surrey,
Guildford, Surrey GU2 7XH, United Kingdom*

²*Department of Nuclear Physics, RSPHysSE,
Australian National University, Canberra, ACT 0200, Australia*

³*School of Engineering, University of Brighton,
Brighton, BN2 4GJ, United Kingdom*

⁴*Department of Physics and Astronomy,
University of Manchester, M13 9PL, United Kingdom*

⁵*SF7 Hahn-Meitner Institute, Glienicke Straße 100, D-14104 Berlin, Germany*

⁶*Department of Technical Physics, Peking University, Beijing 100871, China*

(Dated: September 14, 2005)

Abstract

The structure of the deformed, doubly odd nuclide ^{180}Re has been studied by γ -ray and conversion-electron spectroscopy using the $^{174}\text{Yb}(^{11}\text{B},5n)$ reaction with a pulsed 71 MeV beam of ^{11}B ions. Several of the previously known intrinsic states have been given revised spin and parity assignments. Rotational bands are observed with $K^\pi = (4^+), (5^-), (7^+), 8^+, 9^-, 13^+, 14^-, 15^-, 16^+, 21^-$ and (22^+) . Among these, a 4-quasiparticle t -band is identified, which is already energetically favored at its bandhead compared to the corresponding two-quasiparticle band; and two 6-quasiparticle bands are identified and associated with a $\tau = 13 \mu\text{s}$ isomer. The observed structures, including g -factors and alignments, are interpreted with the aid of Nilsson-plus-BCS calculations and configuration-constrained potential-energy-surface calculations. Reduced hindrance values are obtained for K-forbidden transitions, illustrating the important role of the K quantum number for near-yrast isomers.

PACS numbers: 23.20.Lv, 27.70.+q, 21.10.Tg

*Electronic address: p.walker@surrey.ac.uk

I. INTRODUCTION

The odd-odd deformed nuclide ${}^{180}_{75}\text{Re}_{105}$ is located in the high- Z part of the well deformed $A\sim 160\text{--}180$ region of the Segrè chart. Nuclei in this region have high- K orbitals close to the Fermi surface (where K is the spin projection on the symmetry axis). Broken-pair states at modest excitation energies can have high K values and are able to compete with collective rotation in the formation of the yrast line (the locus of states with lowest energy as a function of spin) [1, 2]. The approximate conservation of the K quantum number then leads to long-lived isomers, exemplified by the $\tau = 45$ -year mean-life of a $K^\pi = 16^+$, 4-quasiparticle isomer in ${}^{178}_{72}\text{Hf}_{106}$ [3]. However, for different nucleon numbers the mean-lives of multi-quasiparticle states are seen to decrease rapidly, due to a combination of less-favorable energetics and increased K mixing [2]. Considering quasiparticle numbers ≥ 4 in the $Z=76$ osmium isotopes, for example, the longest-lived isomers have mean-lives in the ns range, while μs isomers are known in the $Z=75$ rhenium isotopes ${}^{179}\text{Re}$ [4] and ${}^{181}\text{Re}$ [5]. The present work is concerned with the study of isomers and associated structures in their odd-odd neighbor ${}^{180}\text{Re}$, which could give additional information about the robustness of the K quantum number.

Low-spin states in ${}^{180}\text{Re}$ have been studied previously through the electron-capture decay of ${}^{180}\text{Os}$ [6–9]. The ${}^{180}\text{Re}$ ground state is unstable, with $\tau = 3.5$ minutes and a tentative spin and parity of $(1)^-$. It decays by electron capture to the stable nuclide ${}^{180}\text{W}$. The high-spin states of ${}^{180}\text{Re}$ have been investigated twice [10, 11] in the past two decades, but the experiments failed to agree on common spin, parity and configuration assignments, even for the low-lying states. The first experiment [10] used the ${}^{176}\text{Yb}({}^{10}\text{B},6\text{n})$ reaction and obtained a level scheme up to high spin in which five rotational bands were identified and interpreted as being part of ${}^{180}\text{Re}$, even though there were no connections with the low-spin part of the level scheme [8, 9]. A 4-quasiparticle isomer was also reported, with associated rotational bands. The second high-spin experiment [11] used two different beam and target combinations, ${}^{181}\text{Ta}(\alpha,5\text{n})$ and ${}^{170}\text{Er}({}^{14}\text{N},4\text{n})$, and established the existence of six strongly coupled rotational bands and a seventh band which showed a significant energy splitting between the sequences of different signature. The 4-quasiparticle isomer was confirmed and higher-lying isomers were reported but not characterised. Again, connections with the low-spin states were not identified, and spin assignments remained tentative. The interpretations

of the two data sets [10, 11] differed substantially.

The structures of the 2-quasiparticle bands have been reinterpreted by Jain et al. [12]. The present work builds on this, reports new connections between the known bands, extends those bands to higher spin, and identifies two 6-quasiparticle bands for the first time. Despite these successes, connections with the low-spin states, populated in electron-capture decay, remain unidentified. Nevertheless, a consistent understanding of the high-spin level structure is provided, up to spin values of almost $30 \hbar$. The highest-lying isomer, with $\tau=13\pm 1 \mu\text{s}$, is assigned an $I^\pi=K^\pi=21^-$ six-quasiparticle structure. Its K-forbidden decay provides insight into the persistence of the K quantum number. The present work supersedes a preliminary report [13] of the 4- and 6-quasiparticle results.

II. EXPERIMENTAL PROCEDURE

The nuclide ^{180}Re was populated up to spin $\sim 30 \hbar$ with a 71 MeV beam of ^{11}B ions incident on a self-supporting ^{174}Yb target of thickness 5 mg/cm^2 . The choice of beam energy was based on calculations using the code PACE [14], and by inspection of the experimental γ -ray spectra at different beam energies. Although the evaporation of five neutrons constituted the main channel at 71 MeV, γ rays from other nuclides were also observed, principally ^{181}Re and ^{179}Re , via the 4n and 6n channels, respectively. The γ -ray measurements were made using the CAESAR detector array [15], consisting of six Compton-suppressed n-type coaxial HPGe detectors (with a BGO shield surrounding each detector) mounted at angles of $\pm 48^\circ$, $\pm 97^\circ$ and $\pm 145^\circ$ with respect to the beam axis, and two small-volume unsuppressed planar Ge detectors (LEPS) at $\pm 45^\circ$ used for enhanced sensitivity to low-energy γ rays and X-rays. The array was operated in both singles and coincidence mode.

For measuring conversion electrons, the Super-e electron spectrometer [16] was used, consisting of a superconducting magnet transporter and a Si(Li) detector with an antipositron baffle. This was operated in lens mode, with the baffle system restricting the momentum acceptance. In the current work, two electron-energy ranges were studied, 200–900 keV, and 400–600 keV. To measure the γ -ray spectrum simultaneously with the conversion electrons, a Compton-suppressed HPGe detector was installed at 135° to the beam direction. Efficiency and energy calibrations were performed for each of the two experimental arrangements (CAESAR and Super-e) using a ^{152}Eu radioactive source at the target position.

A. Gamma-ray Measurements

Gamma-gamma coincidence measurements were performed with 1 ns beam pulses, 1.7 μ s apart. A total of 3×10^8 coincidence events were sorted into a variety of 4096×4096 -channel matrices. For example, one matrix had the requirement that the γ rays occur within ± 40 ns of each other. Another had the time relationship relaxed to ± 170 ns, thus including low-energy γ rays and X-rays, which can experience considerable time walk. Additional conditions that the events occur during the beam pulses, or between beam pulses, have been used. To study across-isomer correlations *early-delayed* matrices were constructed in two time-difference regimes, 40-170 ns and 170-800 ns. Projection of those events that precede an isomer was achieved by gating on transitions that follow it, and vice versa.

Two three-dimensional matrices (cubes) were sorted for detailed time analysis. For states depopulated by low-energy γ rays, a γ -X- Δt cube was constructed, with HPGe-detector events on one axis, LEPS events on the second axis, and the time difference between them on the third axis. A corresponding γ - γ - Δt cube was also constructed. The background-subtracted spectra were then obtained by projecting onto the time axis with gates on the γ -rays which populated and depopulated the levels of interest. This enabled lifetimes in the $ns \rightarrow \mu s$ range to be associated with specific states.

In order to measure longer lifetimes, separate measurements were performed with two different μs -pulsing ranges. One was with the beam on for 7 μs and off for 107 μs , and the other with the beam on for 53 μs and off for 802 μs . Gamma-ray energies and their times relative to the beam pulses were recorded in event-by-event mode, and two-dimensional γ -time matrices were created.

The DCO (Directional Correlation of Oriented states) technique was used to aid spin determinations. The DCO ratio may be defined as [17]:

$$R_{DCO} = \frac{I_{\theta_1}^{\gamma^2}(Gate_{\theta_2}^{\gamma^1})}{I_{\theta_2}^{\gamma^2}(Gate_{\theta_1}^{\gamma^1})} \quad (1)$$

where I represents the γ -ray intensity, and θ_1 and θ_2 are the angles between each detector and the beam axis. DCO ratios were extracted for the present geometry with $\theta_1 = 145^\circ$, and $\theta_2 = 97^\circ$. If the two transitions in the cascade have the same multipolarity, then gating on either of them gives $R_{DCO} \approx 1$. However, gating on a stretched quadrupole transition gives $R_{DCO} \approx 0.56$ for a stretched dipole transition, and values ranging from $R_{DCO} \approx 0.3$ to ≈ 1.2

for mixed M1/E2 transitions, depending on the spin change and the size and sign of the mixing ratio. Measured DCO ratios are included in table I.

B. Conversion-electron Measurements

The conversion-electron experiment was carried out using a pulsed beam, with 7 μ s pulses separated by 107 μ s. Data were collected only in the off-beam period with the Si(Li) and HPGe detectors, and sorted into two matrices, one with electron energy against the time of arrival relative to the beam pulse, and the other with the γ -ray energy against time.

The electron events were subjected to momentum-selection criteria [16]. After recording the full electron spectrum from the Si(Li) detector, events were selected which satisfy the defined relationship between the electron energy and the solenoid field. The energy-dependent time response of electrons and γ rays was corrected, and matched spectra were produced. Conversion coefficients were obtained directly from the ratios of efficiency-corrected electron and γ -ray intensities.

III. EXPERIMENTAL RESULTS

Eleven rotational bands have been identified in the present work, based on 2-, 4-, and 6-quasiparticle configurations. The level scheme is presented in two parts. Figure 1 shows 2-quasiparticle bands 1, 2 and 3, and Figure 2 shows 2-quasiparticle bands 3, 4 and 11 together with the 4- and 6-quasiparticle bands. For clarity, band 3 is reproduced in both figures. The γ -ray energies and intensities for transitions assigned to ^{180}Re are listed in Table I, while conversion coefficients are listed in Table II. Representative singles spectra for conversion electrons and γ -rays are shown in Figure 3. In addition to the conversion coefficients obtained directly from the ratio of the electron and γ -ray intensities, for low-energy transitions the total conversion coefficients have been extracted from transition intensity balances. The coefficients are compared with theoretical values [18] to distinguish between electric and magnetic characters. According to the general behavior of γ -ray transition probabilities, only E1, M1 and E2 multipolarities need to be considered, except for transitions depopulating bandheads where significant lifetimes are measured. Strongly populated bands are assumed to be closer to yrast than more weakly populated bands. The K value of a rotational band

is usually taken to be the spin of the bandhead. An exception to this rule arises for bands 1 and 2, where the K value is taken to be lower than the bandhead spin by $2\hbar$ and $1\hbar$, respectively (see later).

The level scheme presented in Figures 1 and 2 takes as its starting point bands 4 and 11, interpreted by Jain et al. [12] to have $K^\pi = 8^+$ and $K^\pi = 9^-$, respectively. In ref. [12] a series of arguments was used to modify assignments given previously [10, 11]. Jain et al. [12] considered signature splittings, g -factors, systematics from neighboring nuclei, bandhead energies (including residual interactions) and quasiparticle alignments, to establish reliable and consistent configurations for these 2-quasiparticle bands. Our experimental and theoretical results (see Section IV) for bands 4 and 11 are in good accord with the conclusions of Jain et al., and hence these two bands used as the foundation for constructing the rest of the level scheme. Although they do not have experimental spin assignments, their structures and spins are considered to be on firm ground, and parentheses are not used for their spins and parities in the following presentation. Rather, parentheses are used to distinguish assignments that are tentative *relative* to bands 4 and 11.

Nilsson configuration assignments are suggested in the following sections for each of the observed rotational bands. These are proposed with the aid of multi-quasiparticle calculations (discussed later) and in each case care is taken that the configuration should be consistent both with the degree of rotational alignment and with the experimental g -factors. Plots of alignment as a function of rotational frequency are shown in Figure 4. Configurations which involve $i_{13/2}$, $9/2^+[624]$ neutrons and $h_{9/2}$, $1/2^-[541]$ protons are strongly affected by the Coriolis force and have relatively large alignments at low rotational frequency.

The in-band γ -ray branching ratios have been used to determine g_K values from the rotational-model expressions:

$$\frac{\delta^2}{1 + \delta^2} = \frac{2K^2(2I - 1)}{(I + 1)(I + K - 1)(I - K - 1)} \left(\frac{E_1}{E_2}\right)^5 \lambda, \quad (2)$$

$$\frac{g_K - g_R}{Q_0} = \frac{0.933E_1}{\delta\sqrt{I^2 - 1}} \quad (3)$$

where δ is the $E2/M1$ mixing ratio, E is the transition energy in MeV, λ is the $(\Delta I = 2)/(\Delta I = 1)$ γ -ray transition intensity ratio, and g_R is the rotational g -factor. Q_0 is the intrinsic quadrupole moment given in units of e.b. For all bands in ^{180}Re , $Q_0 = 5.6 \pm 0.5$ e.b

TABLE I: Gamma-ray energy, relative intensity, initial and final level energy, initial and final spin and parity, and DCO ratio, for transitions assigned to ^{180}Re . Tentative assignments and uncertainties are given in parentheses.

E_γ (keV)	I_γ^a	E_i	E_f^b	$K, I_i^\pi \rightarrow K, I_f^\pi$	R_{DCO}^c
42.4(3)	73(27)	205.3	163.0	8, 8 ⁺ (7, 8 ⁺)	
45.8(5)	177(29)	45.8	0.0	(4, 6 ⁺) (4, 5 ⁺)	
54.8(5)	56(28)	1755.2	1700.4	15, 15 ⁻ 14, 14 ⁻	
(62.9)	w ^d	3471.3	3408.4	21, 21 ⁻ (18, 20 ⁺)	
77.5(2)	36(12)	123.3	45.8	(4, 7 ⁺) (4, 6 ⁺)	
79.1(2)	20(4)	284.4	205.3	9, 9 ⁻ 8, 8 ⁺	
(85.4)	w ^d	1755.2	1669.8	15, 15 ⁻ (13, 13 ⁻)	
88.5(2)	70(17)	266.3	177.8	(5, 8 ⁻) (5, 7 ⁻)	
92.2(6)	85(12)	163.0	70.8	(7, 8 ⁺) (7, 7 ⁺)	0.87(12)
102.2(1)	21(10)	3471.3	3369.1	21, 21 ⁻ (19, 19 ⁻)	
104.1(1)	79(18)	370.9	266.3	(5, 9 ⁻) (5, 8 ⁻)	0.96(14)
106.3(5)	72(20)	230.1	123.3	(4, 8 ⁺) (4, 7 ⁺)	
120.5(1)	334(73)	1875.7	1755.2	16, 16 ⁺ 15, 15 ⁻	
121.4(2)	766(218)	284.4	163.0	9, 9 ⁻ (7, 8 ⁺)	
(132.0(3)	45(14)	177.8	45.8	5, 7 ⁻ 4, 6 ⁺)	
133.2(2)	24(5)	362.9	230.1	(4, 9 ⁺) (4, 8 ⁺)	
134.1(4)	160(17)	1700.4	1566.3	14, 14 ⁻ 13, 13 ⁺	
134.3(4)	99(29)	418.7	284.4	9, 10 ⁻ 9, 9 ⁻	0.89(1)
134.5(2)	605(148)	205.3	70.8	8, 8 ⁺ (7, 7 ⁺)	
141.4(2)	38(10)	1566.3	1424.8	13, 13 ⁺ 8, 13 ⁺	
145.3(1)	37(8)	672.6	526.6	(5, 11 ⁻) (5, 10 ⁻)	
149.5(4)	218(22)	312.5	163.0	(7, 9 ⁺) (7, 8 ⁺)	0.96(3)
155.7(1)	248(15)	526.6	370.9	(5, 10 ⁻) (5, 9 ⁻)	
159.8(1)	22(5)	523.1	362.9	(4, 10 ⁺) (4, 9 ⁺)	
163.1(8)	60(8)	1566.3	1403.2	13, 13 ⁺ (12, 12 ⁻)	
173.4(3)	17(8)	696.2	523.1	(4, 11 ⁺) (4, 10 ⁺)	

TABLE I CONTINUED

E_γ (keV)	I_γ^a	E_i^b	E_f	$K, I_i^\pi \rightarrow K, I_f^\pi$	R_{DCO}^c
176.8(2)	211(17)	595.4	418.7	9, 11 ⁻ 9, 10 ⁻	0.96(4)
177.1(6)	51(6)	1079.8	902.4	(5, 13 ⁻) (5, 12 ⁻)	
182.5(6)	154(29)	495.0	312.5	(7, 10 ⁺) (7, 9 ⁺)	1.04(4)
184.3(1)	34(11)	230.1	45.8	(4, 8 ⁺) (4, 6 ⁺)	1.01(4)
193.1(2)	47(10)	370.9	177.8	(5, 9 ⁻) (5, 7 ⁻)	
199.8(3)	31(13)	1586.3	1387.0	(5, 15 ⁻) (5, 14 ⁻)	
201.2(8)	60(6)	696.2	495.0	(4, 11 ⁺) (7, 10 ⁺)	
208.6(2)	377(14)	413.9	205.3	8, 9 ⁺ 8, 8 ⁺	0.85(4)
209.9(4)	319(13)	805.3	595.4	9, 12 ⁻ 9, 11 ⁻	0.91(5)
210.6(4)	26(13)	523.1	312.5	(4, 10 ⁻) (7, 9 ⁺)	
220.5(1)	28(4)	715.5	495.0	(7, 11 ⁺) (7, 10 ⁺)	
228.4(4)	347(29)	642.3	413.9	8, 10 ⁺ 8, 9 ⁺	1.07(2)
229.1(2)	68(11)	1929.5	1700.4	(14, 15 ⁻) (14, 14 ⁻)	0.95(12)
229.9(1)	133(28)	902.4	672.6	5, 12 ⁻ 5, 11 ⁻	
231.4(3)	55(25)	2160.9	1929.5	14, 16 ⁻ 14, 15 ⁻	0.83(14)
233.6(2)	32(6)	949.1	715.5	(7, 12 ⁺) (7, 11 ⁺)	
237.4(2)	207(16)	1042.7	805.3	9, 13 ⁻ 9, 12 ⁻	
239.6(1)	74(10)	362.9	123.3	(4, 9 ⁺) (4, 7 ⁺)	0.96(8)
241.8(1)	55(5)	312.5	70.8	(7, 9 ⁺) (7, 7 ⁺)	
245.9(5)	293(26)	888.2	642.3	8, 11 ⁺ 8, 10 ⁺	0.95(2)
252.9(3)	23(10)	949.1	696.2	(7, 12 ⁺) (4, 11 ⁺)	
255.5(1)	82(13)	1204.6	949.1	(7, 13 ⁺) (7, 12 ⁺)	
259.5(2)	87(37)	2420.4	2160.9	14, 17 ⁻ 14, 16 ⁻	
260.3(2)	124(33)	526.6	266.3	(5, 10 ⁻) (5, 8 ⁻)	
261.1(4)	96(9)	1303.9	1042.7	9, 14 ⁻ 9, 13 ⁻	0.85(6)
261.4(5)	308(35)	1149.6	888.2	8, 12 ⁺ 8, 11 ⁺	0.96(3)
262.4(2)	38(7)	1566.3	1303.9	13, 13 ⁺ 9, 14 ⁻	
263.9(1)	299(15)	2139.6	1875.7	16, 17 ⁺ 16, 16 ⁺	0.94(2)
275.2(1)	139(23)	1424.8	1149.6	8, 13 ⁺ 8, 12 ⁺	1.20(4)

TABLE I CONTINUED

E_γ (keV)	I_γ^a	E_i^b	E_f	$K, I_i^\pi \rightarrow K, I_f^\pi$	R_{DCO}^c
275.9(1)	248(52)	2415.5	2139.6	16, 18 ⁺ 16, 17 ⁺	1.06(2)
277.3(4)	33(16)	1481.9	1204.6	(7, 14 ⁺) (7, 13 ⁺)	
(280.2(2)	56(24)	1846.5	1566.3	13, 14 ⁺ 13, 13 ⁺)	
283.2(6)	30(20)	1587.0	1303.9	9, 15 ⁻ 9, 14 ⁻	0.79(5)
285.7(1)	60(20)	3408.4	3122.4	(18, 20 ⁺) (18, 18 ⁺)	
285.9(4)	42(13)	1767.8	1481.9	(7, 15 ⁺) (7, 14 ⁺)	
287.2(4)	42(19)	1712.0	1424.8	8, 14 ⁺ 8, 13 ⁺	0.97(8)
289.9(2)	121(46)	2710.4	2420.4	14, 18 ⁻ 14, 17 ⁻	1.00(3)
290.0(1)	44(14)	2045.2	1755.2	15, 16 ⁻ 15, 15 ⁻	1.09(5)
291.1(1)	22(5)	2706.7	2415.5	16, 19 ⁺ 16, 18 ⁺	0.85(0.4)
292.1(4)	56(26)	3002.5	2710.4	14, 19 ⁻ 14, 18 ⁻	
293.0(2)	67(22)	523.1	230.1	(4, 10 ⁺) (4, 8 ⁺)	1.15(7)
295.9(2)	49(9)	2007.8	1712.0	8, 15 ⁺ 8, 14 ⁺	
300.3(6)	65(7)	2375.4	2075.0	(7, 17 ⁺) (7, 16 ⁺)	
(300.5(4)	25(10)	3369.1	3068.6	19, 19 ⁻ 18, 18 ⁺)	
301.0(1)	75(8)	1888.1	1587.0	9, 16 ⁻ 9, 15 ⁻	0.69(7)
(301.6(2)	w ^d	2148.1	1846.5	13, 15 ⁺ 13, 14 ⁺)	
301.7(4)	9(8)	672.6	370.9	(5, 11 ⁻) (5, 9 ⁻)	
301.8(1)	111(13)	2309.6	2007.8	8, 16 ⁺ 8, 15 ⁺	
305.1(3)	31(7)	2921.9	2616.8	8, 18 ⁺ 8, 17 ⁺	
307.1(1)	97(11)	2616.8	2309.6	8, 17 ⁺ 8, 16 ⁺	
307.2(6)	62(6)	2075.0	1767.8	(7, 16 ⁺) (7, 15 ⁺)	
307.4(2)	69(24)	3014.1	2706.7	16, 20 ⁺ 16, 19 ⁺	0.98(6)
307.8(3)	90(31)	1387.0	1079.8	(5, 14 ⁻) (5, 13 ⁻)	
310.9(2)	10(20)	3861.4	3550.5	9, 22 ⁻ 9, 21 ⁻	
311.0(4)	100(10)	595.4	284.4	9, 11 ⁻ 9, 9 ⁻	
311.0(2)	62(22)	2356.2	2045.2	15, 17 ⁻ 15, 16 ⁻	0.99(5)
312.1(3)	29(9)	3234.0	2921.9	(8, 19 ⁺) 8, 18 ⁺	
316.9(2)	35(13)	2205.0	1888.1	9, 17 ⁻ 9, 16 ⁻	0.77(8)

TABLE I CONTINUED

E_γ (keV)	I_γ^a	E_i^b	E_f	$K, I_i^\pi \rightarrow K, I_f^\pi$	R_{DCO}^c
317.7(4)	30(10)	3369.1	3051.4	(19, 19 ⁻) 18, 18 ⁺	
317.9(1)	65(20)	2693.3	2375.4	(7, 18 ⁺) (7, 17 ⁺)	
319.2(4)	w ^d	3002.5	2683.3	14, 19 ⁻ 15, 18 ⁻	
319.6(5)	7(4)	4524.4	4204.8	9, 24 ⁻ 9, 23 ⁻	
323.8(3)	69(24)	3337.9	3014.1	16, 21 ⁺ 16, 20 ⁺	0.90(12)
(324.5(2))	w ^d	2472.6	2148.1	13, 16 ⁺ 13, 14 ⁺)	
325.1(3)	76(30)	3327.6	3002.5	14, 20 ⁻ 14, 19 ⁻	
327.1(2)	62(10)	2683.3	2356.2	15, 18 ⁻ 15, 17 ⁻	1.14(14)
327.3(1)	33(7)	2532.3	2205.0	9, 18 ⁻ 9, 17 ⁻	0.79(16)
331.9(8)	65(7)	495.0	163.0	(7, 10 ⁺) (7, 8 ⁺)	
333.3(1)	65(15)	696.2	362.9	(4, 11 ⁺) (4, 9 ⁺)	1.01(7)
336.9(6)	23(8)	3209.0	2872.1	9, 20 ⁻ 9, 19 ⁻	
339.8(2)	23(4)	2872.1	2532.3	9, 19 ⁻ 9, 18 ⁻	0.79(16)
340.9(2)	42(22)	3668.4	3327.6	14, 21 ⁻ 14, 20 ⁻	
341.0(8)	88(32)	3678.9	3337.9	16, 22 ⁺ 16, 21 ⁺	0.82(11)
341.5(1)	32(5)	3550.5	3209.0	9, 21 ⁻ 9, 20 ⁻	
343.4(6)	24(9)	4204.8	3861.4	9, 23 ⁻ 9, 22 ⁻	
352.6(2)	21(5)	715.5	362.9	(7, 11 ⁺) (4, 9 ⁺)	
356.6(2)	62(25)	4025.1	3668.5	14, 22 ⁻ 14, 21 ⁻	
357.8(2)	38(22)	4036.7	3678.9	16, 23 ⁺ 16, 22 ⁺	1.31(33)
(363.0(2))	w ^d	4887.4	4524.4	9, 25 ⁻ 9, 24 ⁻)	
366.3(3)	23(12)	4391.4	4025.1	14, 23 ⁻ 14, 22 ⁻	
374.0(1)	48(13)	4269.3	3895.3	(22, 23 ⁺) (22, 22 ⁺)	0.94(9)
375.8(1)	142(28)	902.4	526.6	(5, 12 ⁻) (5, 10 ⁻)	
375.8(1)	70(5)	4412.5	4036.7	16, 24 ⁺ 16, 23 ⁺	1.02(2)
380.0(4)	41(8)	3851.3	3471.3	21, 22 ⁻ 21, 21 ⁻	
381.9(1)	30(11)	4651.2	4269.3	(22, 24 ⁺) (22, 23 ⁺)	1.08(18)
382.4(1)	174(30)	905.5	523.1	(4, 12 ⁺) (4, 10 ⁺)	1.09(5)
382.5(3)	74(25)	1969.2	1586.3	(5, 16 ⁻) (5, 15 ⁻)	

TABLE I CONTINUED

E_γ (keV)	I_γ^a	E_i^b	E_f	$K, I_i^\pi \rightarrow K, I_f^\pi$	R_{DCO}^c
383.7(6)	20(7)	696.2	312.5	(4, 11 ⁺) (7, 9 ⁺)	
386.7(6)	69(7)	805.3	418.7	9, 12 ⁻ 9, 10 ⁻	1.34(8)
388.7(2)	15(6)	5039.9	4651.2	(22, 25 ⁺) (22, 24 ⁺)	
389.5(4)	67(10)	4802.0	4412.5	16, 25 ⁺ 16, 24 ⁺	
389.5(2)	19(12)	4240.8	3851.3	21, 23 ⁻ 21, 22 ⁻	
395.7(3)	11(5)	5435.6	5039.9	(22, 26 ⁺) (22, 25 ⁺)	
396.6(1)	36(19)	4637.5	4240.8	21, 24 ⁻ 21, 23 ⁻	1.12(17)
402.5(6)	6(4)	5838.1	5435.6	(22, 27 ⁺) (22, 26 ⁺)	
403.4(2)	38(7)	715.5	312.5	(7, 11 ⁺) (7, 9 ⁺)	
404.2(2)	w ^d	5206.2	4802.0	16, 26 ⁺ 16, 25 ⁺	
407.2(2)	100(10)	1079.8	672.6	(5, 13 ⁻) (5, 11 ⁻)	
407.2(3)	4.0(20)	5455.2	5047.9	21, 26 ⁻ 21, 25 ⁻	
410.5(2)	45(8)	905.5	495.0	(4, 12 ⁻) (7, 10 ⁺)	
410.5(5)	45(20)	5047.9	4637.5	21, 25 ⁻ 21, 24 ⁻	
411.7(4)	w ^d	6249.6	5838.1	(22, 28 ⁺) (22, 27 ⁺)	
416.3(1)	54(11)	1131.8	715.5	(4, 13 ⁺) (7, 11 ⁺)	
416.6(4)	198(15)	1566.3	1149.6	13, 13 ⁺ 8, 12 ⁺	
423.7(2)	w ^d	6673.5	6249.8	(22, 29 ⁺) (22, 28 ⁺)	
424.0(2)	107(11)	3895.3	3471.3	(22, 22 ⁺) 21, 21 ⁻	
435.6(1)	102(23)	1131.8	696.2	(4, 13 ⁺) (4, 11 ⁺)	1.01(5)
437.0(4)	45(16)	642.3	205.3	8, 10 ⁺ 8, 8 ⁺	
447.3(4)	121(11)	1042.7	595.4	9, 13 ⁻ 9, 11 ⁻	1.39(8)
454.1(6)	55(17)	949.1	495.0	(7, 12 ⁺) (7, 10 ⁺)	1.30(18)
456.8(6)	118(10)	3471.3	3014.1	21, 21 ⁻ 16, 20 ⁺	
460.6(2)	46(21)	2160.9	1700.4	14, 16 ⁻ 14, 14 ⁻	1.11(18)
473.6(6)	138(32)	1379.1	905.5	(4, 14 ⁺) (4, 12 ⁺)	0.99(5)
474.3(8)	163(19)	888.2	413.9	8, 11 ⁺ 8, 9 ⁺	1.17(5)
484.6(1)	283(63)	1387.0	902.4	(5, 14 ⁻) (5, 12 ⁻)	
489.2(2)	55(10)	1204.6	715.5	(7, 13 ⁺) (7, 11 ⁺)	

TABLE I CONTINUED

E_γ (keV)	I_γ^a	E_i^b	E_f	$K, I_i^\pi \rightarrow K, I_f^\pi$	R_{DCO}^c
491.7(5)	18(19)	2420.4	1929.5	14, 17 ⁻ 14, 15 ⁻	0.81(8)
498.6(4)	117(11)	1303.9	805.3	9, 14 ⁻ 9, 12 ⁻	
506.5(2)	158(44)	1586.3	1079.8	(5, 15 ⁻) (5, 13 ⁻)	
507.4(3)	92(22)	1149.6	642.3	8, 12 ⁺ 8, 10 ⁺	
508.4(2)	8(2)	1204.6	696.2	(7, 13 ⁺) (4, 11 ⁺)	
511.3(1)	72(17)	1643.1	1131.8	(4, 15 ⁺) (4, 13 ⁺)	0.99(5)
523.5(1)	60(9)	1566.3	1042.7	13, 13 ⁺ 9, 13 ⁻	
532.7(2)	51(10)	1481.9	949.1	(7, 14 ⁺) (7, 12 ⁺)	
536.6(2)	66(13)	1424.8	888.2	8, 13 ⁺ 8, 11 ⁺	
539.7(3)	40(22)	2415.5	1875.7	16, 18 ⁺ 16, 16 ⁺	1.25(16)
544.3(4)	128(10)	1587.0	1042.7	9, 15 ⁻ 9, 13 ⁻	
547.3(1)	95(24)	1926.4	1379.1	(4, 16 ⁺) (4, 14 ⁺)	
548.2(1)	26(21)	2710.3	2160.9	14, 18 ⁻ 14, 16 ⁻	1.06(13)
562.3(3)	38(13)	1712.0	1149.6	8, 14 ⁺ 8, 12 ⁺	
563.2(2)	73(4)	1767.8	1204.6	(7, 15 ⁺) (7, 13 ⁺)	
567.0(3)	28(16)	2706.7	2139.6	16, 19 ⁺ 16, 17 ⁺	1.18(25)
579.4(2)	52(16)	2222.5	1643.1	(4, 17 ⁺) (4, 15 ⁺)	
581.5(1)	46(19)	3002.5	2420.4	14, 19 ⁻ 14, 17 ⁻	1.39(44)
(581.8(2)	w ^d	2148.1	1566.3	13, 15 ⁺ 13, 13 ⁺)	
582.2(4)	96(53)	1969.2	1387.0	(5, 16 ⁻) (5, 14 ⁻)	1.38(19)
583.0(3)	67(16)	2007.8	1424.8	8, 15 ⁺ 8, 13 ⁺	
584.2(1)	89(13)	1888.1	1303.9	9, 16 ⁻ 9, 14 ⁻	
593.2(3)	47(11)	2075.0	1481.9	(7, 16 ⁺) (7, 14 ⁺)	1.37(17)
597.7(4)	80(20)	2309.6	1712.0	8, 16 ⁺ 8, 14 ⁺	
599.7(3)	64(33)	3014.1	2415.5	16, 20 ⁺ 16, 18 ⁺	0.92(22)
600.2(2)	155(61)	2186.5	1586.3	(5, 17 ⁻) (5, 15 ⁻)	
601.0(2)	w ^d	2356.2	1755.2	15, 17 ⁻ 15, 15 ⁻	
607.6(6)	107(13)	2375.4	1767.8	(7, 17 ⁺) (7, 15 ⁺)	1.25(18)
609.0(1)	167(22)	2616.8	2007.8	8, 17 ⁺ 8, 15 ⁺	

TABLE I CONTINUED

E_γ (keV)	I_γ^a	E_i^b	E_f	$K, I_i^\pi \rightarrow K, I_f^\pi$	R_{DCO}^c
610.6(2)	83(28)	2537.0	1926.4	(4, 18 ⁺) (4, 16 ⁺)	
612.2(2)	123(18)	2921.9	2309.6	8, 18 ⁺ 8, 16 ⁺	
616.9(4)	40(33)	3327.6	2710.4	14, 20 ⁻ 14, 18 ⁻	1.24(16)
617.2(1)	158(21)	3234.0	2616.8	(8, 19 ⁺) 8, 17 ⁺	
618.2 (2)	w ^d	2693.3	2075.0	(7, 18 ⁺) (7, 16 ⁺)	
618.3(8)	97(10)	2205.0	1587.0	9, 17 ⁻ 9, 15 ⁻	
(626.1(2)	w ^d	2472.6	1846.5	13, 16 ⁺ 13, 14 ⁺)	
631.9(5)	50(47)	3337.9	2706.7	16, 21 ⁺ 16, 19 ⁺	0.85(18)
638.1(1)	28(11)	2683.3	2045.2	15, 18 ⁻ 15, 16 ⁻	
638.2(2)	39(15)	2860.7	2222.5	(4, 19 ⁺) (4, 17 ⁺)	
644.5(6)	70(7)	2532.3	1888.1	9, 18 ⁻ 9, 16 ⁻	
651.6(6)	23(4)	3861.4	3209.0	9, 22 ⁻ 9, 20 ⁻	
654.8(2)	21(4)	4204.8	3550.5	9, 23 ⁻ 9, 21 ⁻	
663.0(4)	20(9)	4524.4	3861.4	9, 24 ⁻ 9, 22 ⁻	
664.1(2)	49(29)	2633.3	1969.2	(5, 18 ⁻) (5, 16 ⁻)	
665.5(1)	74(34)	3678.9	3014.1	16, 22 ⁺ 16, 20 ⁺	1.02(18)
665.9(2)	69(20)	3202.9	2537.0	(4, 20 ⁺) (4, 18 ⁺)	
666.0 (4)	w ^d	3668.4	3002.5	14, 21 ⁻ 14, 19 ⁻	1.18(7)
667.1(1)	62(7)	2872.1	2205.0	9, 19 ⁻ 9, 17 ⁻	
676.9(4)	45(8)	3209.0	2532.3	9, 20 ⁻ 9, 18 ⁻	
678.1(1)	169(23)	1566.3	888.2	13, 13 ⁺ 8, 11 ⁺	
679.3(2)	44(5)	3550.5	2872.1	9, 21 ⁻ 9, 19 ⁻	
681.2(3)	55(33)	2867.7	2186.5	(5, 19 ⁻) (5, 17 ⁻)	
(682.6(4)	10(4)	4887.4	4204.8	9, 25 ⁻ 9, 23 ⁻)	
689.1(2)	w ^d	3549.8	2860.7	(4, 21 ⁺) (4, 19 ⁺)	0.97(5)
696.5(1)	48(33)	4025.1	3327.6	14, 22 ⁻ 14, 20 ⁻	1.24(12)
698.7(2)	w ^d	4036.7	3337.9	16, 23 ⁺ 16, 21 ⁺	0.94(16)
707.6(6)	22(10)	3910.5	3202.9	(4, 22 ⁺) (4, 20 ⁺)	
720.0(2)	w ^d	3353.3	2633.3	(5, 20 ⁻) (5, 18 ⁻)	

TABLE I CONTINUED

E_γ (keV)	I_γ^a	E_i^b	E_f	$K, I_i^\pi \rightarrow K, I_f^\pi$	R_{DCO}^c
724.1(5)	56(28)	4391.3	3668.4	14, 23 ⁻ 14, 21 ⁻	1.08(25)
731.8(2)	w ^d	4412.5	3678.9	16, 24 ⁺ 16, 22 ⁺	0.98(17)
732.7(5)	20(10)	4643.2	3910.5	(4, 24 ⁺) (4, 22 ⁺)	0.98(17)
748.4(2)	w ^d	3616.1	2867.7	(5, 21 ⁻) (5, 19 ⁻)	
750.1(2)	w ^d	4299.9	3549.8	(4, 23 ⁺) (4, 21 ⁺)	
756.1(3)	7(4)	4651.2	3895.3	(22, 24 ⁺) (22, 22 ⁺)	
761.0(1)	38(5)	1566.3	805.3	13, 13 ⁺ 9, 12 ⁻	
764.2(2)	w ^d	4802.0	4036.7	16, 25 ⁺ 16, 23 ⁺	
768.3(5)	12(10)	4240.8	3471.3	21, 23 ⁻ 21, 21 ⁻	
771.2(4)	7(4)	5039.9	4269.3	(22, 25 ⁺) (22, 23 ⁺)	
784.2(4)	7(3)	5435.6	4651.2	(22, 26 ⁺) (22, 24 ⁺)	
786.8(3)	7(5)	4637.5	3851.3	21, 24 ⁻ 21, 22 ⁻	
794.1(2)	w ^d	5206.2	4412.5	16, 26 ⁺ 16, 24 ⁺	
796.0(2)	w ^d	4412.1	3616.1	(5, 23 ⁻) (5, 21 ⁻)	
797.7(3)	8(4)	5838.1	5039.9	(22, 27 ⁺) (22, 25 ⁺)	
799.2(4)	4(3)	5047.9	4240.8	21, 25 ⁻ 21, 23 ⁻	
(802.7(2)	w ^d	5102.6	4299.9	4, 25 ⁺ 4, 23 ⁺)	
807.8(6)	19(7)	1403.2	595.4	(12, 12 ⁻) 9, 11 ⁻	
809.2(4)	4(3)	5455.2	4637.5	21, 26 ⁻ 21, 24 ⁻	
813.5(6)	6(2)	6249.8	5435.6	(22, 28 ⁺) (22, 26 ⁺)	
835.6(6)	3(2)	6673.5	5838.1	(22, 29 ⁺) (22, 27 ⁺)	
895.3(8)	8(2)	1700.4	805.3	14, 14 ⁻ 9, 12 ⁻	
912.2(3)	13(3)	3051.4	2139.6	18, 18 ⁺ 16, 17 ⁺	
929.0(2)	15(2)	3068.6	2139.6	(18, 18 ⁺) 16, 17 ⁺	
982.8(2)	13(3)	3122.4	2139.6	(18, 18 ⁺) 16, 17 ⁺	
984.5(1)	87(13)	1403.2	418.7	(12, 12 ⁻) 9, 10 ⁻	
1074.4(3)	23(10)	1669.8	595.4	(13, 13 ⁻) 9, 11 ⁻	
1164.1(3)	7(2)	3369.1	2205.0	(19, 19 ⁻) 9, 17 ⁻	
1175.8(1)	48(16)	3051.4	1875.7	18, 18 ⁺ 16, 16 ⁺	

TABLE I CONTINUED

E_γ (keV)	I_γ^a	E_i^b	E_f	$K, I_i^\pi \rightarrow K, I_f^\pi$	R_{DCO}^c
1192.9(2)	15(4)	3068.6	1875.7	(18, 18 ⁺) 16, 16 ⁺	
1246.7(1)	41(10)	3122.4	1875.7	(18, 18 ⁺) 16, 16 ⁺	

^a Relative γ -ray intensity with arbitrary normalisation.

^b All energies of levels are relative to the $I^\pi=(5^+)$ bandhead of band 2.

^c DCO ratios (see text).

^d w indicates that the γ -ray intensity is low.

and $g_R=0.30\pm 0.05$ were used, as adopted by Venkova et al. [11]. The subscripts 1,2 refer to $\Delta I=1,2$ transitions. The experimental values are compared with Nilsson-model estimates, using:

$$Kg_K = \sum(\Lambda g_\Lambda + \Sigma g_\Sigma) \quad (4)$$

where Λ and Σ are projections of the orbital and intrinsic spins, respectively, with $g_\Lambda=0$ for neutrons and 1 for protons. The free nucleon values of $g_\Sigma=-3.83$ for neutrons and $+5.59$ for protons are attenuated by a factor of 0.6 [19], and Nilsson-model wavefunctions are used to determine the expectation values of the intrinsic-spin projections. Equation 2 assumes a well defined K value and only yields the magnitude of δ and not its sign. In this work the sign of $(g_K - g_R)$ has not been determined, though positive signs have been previously obtained [11] from γ -ray angular distributions for bands 3, 4, 8 and 11 (with $K^\pi = 7^+, 8^+, 16^+$ and 9^- , respectively). Nevertheless, it is not straightforward to make a quantitative comparison with the resulting g -factors from ref. [11] on account of the different K values that have been used.

The measured $|g_K - g_R|$ values are listed in Table III and compared with corresponding theoretical values. There is reasonable agreement for all assigned bands (though not the unassigned $K^\pi = 4^-$ option) providing support for the suggested configurations. The last column in Table III lists cases where $g_K = 0.08$ is used for $i_{13/2}$ neutrons [19], and $g_K = -1.0$ is used for $h_{9/2}$ protons [20]. These values allow for alignment effects, and typically lead to improved agreement with experimental values. At least part of the remaining discrepancies can be attributed to the assumption of fixed $g_R = 0.30$. As observed for multi-quasiparticle bands in, for example, ^{178}W [21] and ^{179}W [19], there is evidence that the neutron-proton

TABLE II: Conversion coefficients for selected transitions in ^{180}Re

E_γ	Shell	α_{exp}	α_{th}	Multipolarity
42.4	TOT ^{a)}	13(4)	M1: 11.5	M1
54.8	TOT ^{a)}	7(2)	M1: 5.40	M1
77.5	TOT ^{a)}	8.3(3)	M1: 11.3	M1
102.2	TOT ^{a)}	2.5(9)	E2: 3.84	E2
120.5	TOT ^{a)}	0.6(3)	E1: 0.24; M1: 3.17	E1
141.4	TOT ^{a)}	1.9(2)	M1: 2.01	M1
245.9	K	0.231(50)	M1: 0.355; E2: 0.0981	M1/E2
275.9	K	0.190(25)	M1: 0.258; E2: 0.0725	M1/E2
285.7	K	0.077(12)	E2: 0.0662	E2
307.4	K	0.107(20)	M1: 0.194; E2: 0.0547	M1/E2
416.6	K	0.054(6)	M1: 0.0860; E2: 0.0256	M1/E2
447.3	K	0.023(10)	E2: 0.0216	E2
456.8	K	0.0084(10)	E1: 0.00759	E1
474.3	K	0.026(6)	E2: 0.0188	E2
507.4	K	0.020(3)	M1: 0.0514; E2: 0.0161	E2
	L	0.005(2)	M1: 0.00797; E2: 0.00394	
599.7	K	0.012(2)	E2: 0.0112	E2
678.1	K	0.008(1)	E2: 0.00857	E2
1175.8	K	0.003(1)	E2: 0.00287	E2
1192.9	K	0.005(2)	M1: 0.00593; E2: 0.00280	M1 or E2

^{a)} Total conversion coefficient obtained from intensity-balance considerations.

balance in the configuration has a significant influence on g_R . The effect was quantified for the more extensive ^{178}W data set [21], but is not accounted for in the present work.

It is also informative to make comparisons of ^{180}Re band properties (g -factors and alignments) with corresponding bands known [20] in the isotone ^{178}Ta . It is found, for example, that the ^{180}Re low-frequency alignments are systematically $\sim 2 \hbar$ greater than their ^{178}Ta counterparts, a difference which may be understood qualitatively as arising from the smaller β_2 deformation of ^{180}Re , which leads to stronger Coriolis mixing. Specific comparisons are

made in the following sections.

TABLE III: Configurations and average g -factors for 2-, 4- and 6-quasiparticle bands in ^{180}Re .

Band	K^π	Energy (keV)	Configuration ^{a)}	$g_K - g_R$		
				Expt. ^{b)}	Calc. ^{c)}	Calc. ^{d)}
	4^- ^{e)}	178	$\nu 9/2^+ \otimes \pi 1/2^-$	0.45(5)	-0.63	-0.09
1	5^- ^{e)}	178	$\nu 9/2^+ \otimes \pi 1/2^-$	0.35(4)	-0.40	-0.33
2	4^+	0	$\nu 7/2^- \otimes \pi 1/2^-$	0.14(2)	+0.01	-0.22
3	7^+	71	$\nu 9/2^+ \otimes \pi 5/2^+$	0.25(3)	+0.09	+0.27
4	8^+	205	$\nu 7/2^- \otimes \pi 9/2^-$	0.45(5)	+0.50	+0.50
11	9^-	284	$\nu 9/2^+ \otimes \pi 9/2^-$	0.25(3)	+0.22	+0.36
5	13^+	1566	$\nu 7/2^-, 9/2^+, 5/2^- \otimes \pi 5/2^+$		-0.09	+0.01
6	14^-	1700	$\nu 7/2^-, 9/2^+, 7/2^+ \otimes \pi 5/2^+$	0.21(8)	-0.10	+0.06
7	15^-	1755	$\nu 7/2^-, 9/2^+, 5/2^- \otimes \pi 9/2^-$	0.18(9)	+0.01	+0.09
8	16^+	1876	$\nu 7/2^-, 9/2^+, 7/2^+ \otimes \pi 9/2^-$	0.16(3)	-0.01	+0.14
9	21^-	3471	$\nu 7/2^-, 9/2^+, 5/2^- \otimes \pi 5/2^+, 9/2^-, 7/2^+$	0.16(8)	+0.21	+0.27
10	22^+	3895	$\nu 7/2^-, 9/2^+, 7/2^+ \otimes \pi 5/2^+, 9/2^-, 7/2^+$	0.12(6)	+0.19	+0.30

^{a)} ν : $7/2^-$ [514], $7/2^+$ [633], $9/2^+$ [624], $5/2^-$ [512]; π : $1/2^-$ [541], $5/2^+$ [402], $9/2^-$ [514], $7/2^+$ [404].

^{b)} Average values from, at most, the six lowest-spin branching ratios in each band, assuming $Q_0=5.6\pm 0.5$ e.b. The sign of $g_K - g_R$ is not specified experimentally in the present work.

^{c)} Calculated Nilsson-model values with $g_\Sigma = 0.6g_\Sigma^{free}$ and $g_R = 0.30\pm 0.05$.

^{d)} Calculated with $g_K=0.08$ for $7/2^+$ and $9/2^+$ neutrons, and $g_K=-1.0$ for $1/2^-$ protons.

^{e)} Alternative couplings of the same two quasiparticles.

A. Two-quasiparticle Bands

1. Band 4, $K^\pi=8^+$, based on the 205 keV level

Band 4 was observed up to spin (19^+) at 3234 keV. The corresponding bandhead reported in ref. [11] was given a spin assignment of 6^- , in contrast to the 7^+ assignment of Kreiner et al. [10] and the 8^+ assignment of Jain et al. [12]. As indicated above, the Jain et al. 8^+

assignment is adopted here. There are two possible configurations: $\nu 7/2^- [514] \otimes \pi 9/2^- [514]$, and $\nu 9/2^+ [624] \otimes \pi 7/2^+ [404]$. Of these quasiparticles, only the $9/2^+ [624]$ neutron gives substantial alignment. Therefore, the low aligned angular momentum of the observed band at low frequency ($i_x = 2\hbar$ at $\hbar\omega \approx 0.1$ MeV, see Figure 4) favors the former configuration, which has no aligned quasiparticles. The adopted configuration is the same as for the $K^\pi=8^+$ band in ^{178}Ta , which has $|g_K - g_R| = 0.47 \pm 0.05$ [20], compared to the ^{180}Re value of 0.45 ± 0.05 . The alignment shows an initial upbend below $\hbar\omega \approx 0.3$ MeV, which is typically observed in this mass region [22] for $i_{\frac{13}{2}}$ neutron pair breaking. However, a complete alignment was not observed due to the lack of data on higher-spin states for this band. Note that band 8 ($K^\pi=16^+$), which is discussed later, has a related neutron $(i_{\frac{13}{2}})^2$ alignment.

2. Band 11, $K^\pi=9^-$, based on the 284 keV level

Band 11 is assigned a bandhead spin of 9^- , based on the discussion of Jain et al. [12], which is consistent with our results. (Kreiner et al. [10] gave an 8^- assignment, and Venkova et al. [11] gave a 7^+ assignment.) Note that there is a 79 keV transition, assigned E1 character [11], from the 9^- bandhead of band 11 to the 8^+ bandhead of band 4, and all authors agree on the relative spin and parity assignments of bands 4 and 11. Band 11 is now extended to spin (25^-) . The bandhead is isomeric with a measured mean-life of 109 ± 2 ns (see Figure 5). This is consistent with previous results [10, 11], though the uncertainty is now reduced.

Jain et al. [12] gave a configuration assignment of $\nu 9/2^+ [624] \otimes \pi 9/2^- [514]$, which is supported by the present work. The initial alignment (Figure 4) of $i_x = 3.5\hbar$ at $\hbar\omega \approx 0.1$ MeV is consistent with the presence of an $i_{\frac{13}{2}}$ neutron in the configuration. We note that there is competition between the $9/2^+ [624]$ and $7/2^+ [633]$ $i_{\frac{13}{2}}$ neutron orbitals, which are mixed by the Coriolis interaction. However, it is evident from the odd-N isotones ^{179}W [19, 23] and ^{181}Os [24] that the $9/2^+ [624]$ neutron is at slightly lower energy for $N=105$. The band in ^{178}Ta with the same configuration has $|g_K - g_R| = 0.29 \pm 0.03$ [20], similar to the ^{180}Re value of 0.25 ± 0.03 .

The alignment (Figure 4) shows a backbend at $\hbar\omega \approx 0.3$ MeV, which is presumably due to the alignment of a pair of $i_{\frac{13}{2}}$ neutrons. Due to blocking, this alignment should be delayed in frequency relative to bands without an $i_{\frac{13}{2}}$ neutron in the initial configuration. In ^{180}Re ,

there is no good test of this behavior. However, it can be seen that the alignment gain in band 4 ($K^\pi = 8^+$) begins at a lower frequency, as would be expected. Furthermore, these 8^+ and 9^- bands in ^{180}Re have properties that are similar to the corresponding 8^+ and 9^- bands in ^{178}Ta [20].

Additional excited states, found to decay into lower members of band 11, are at 1403 keV (12^-) and 1670 keV (13^-), the latter being newly placed in this work. The 1670 keV state decays via a 1074 keV transition to the 595 keV, $I^\pi=11^-$ level. The $I^\pi=(13^-)$ assignment is implied because, when gating on the 1074 keV transition in the $\gamma-\gamma$ matrix, transitions are seen that feed the 1755 keV, $I^\pi=15^-$ level, which suggests that there is an unobserved and highly converted (E2) 85 keV transition between the $I^\pi=15^-$ state and the state in question. The quasiparticle structures of the 1403 and 1670 keV levels are considered in Section IV.

3. Band 2, $K^\pi=(4^+)$, based on the ground state, and Band 3, $K^\pi=(7^+)$, based on the 71 keV level

Bands 2 and 3 were previously reported in ref. [11]. These two structures are connected by strong interband transitions which help in determining the energy and spin differences. An unobserved 25 keV transition is implied [11], depopulating the bandhead of band 3. Non-observation as a γ -ray is not surprising since an M1, 25 keV transition has a large conversion coefficient ($\alpha_{TOT}=55$). In the present work, a 45.8 keV transition has been established at the bottom of band 2 (see Figure 6). This transition was reported in ref. [10] but not placed in their level scheme.

Band 3 was assigned a 3^- bandhead by Venkova et al. [11]. This clearly conflicts with our connection (see Figure 2) to band 4, which was not identified by Venkova et al. [11], although they inferred the existence of a 42 keV transition on the basis of γ -ray coincidence relationships. Intensity considerations for the 42.4 and 134.5 keV transitions from band 4 to band 3 imply M1 multipolarities, and hence a 7^+ bandhead for the latter. Furthermore, the transitions between bands 2 and 3 can be explained as being due to a crossing of the bands at ≈ 700 keV excitation energy, characterised by chance near degeneracies and wavefunction mixings, as discussed in more detail in Section IV. The crossing requires equal spin and parity values for the 696 and 716 keV levels in the respective bands, and $I^\pi=11^+$ is therefore specified for these two levels to give consistency with the band 3 assignment

already discussed.

Band 2 forms two separate signatures (E2 sequences) above spin 10^+ , in the sense that the $\Delta I=1$ transitions are of too low intensity to be observed. In band 3 on the other hand, the mixed dipole-quadrupole transitions are more intense relative to the stretched E2 transitions. Several additional transitions have been observed in these bands, compared to previous work [10, 11].

Band 3 is assigned the $K^\pi=7^+$, $\nu 9/2^+[624] \otimes \pi 5/2^+[402]$ configuration in accord with ref. [10]. The configuration for band 2 is suggested to be $\nu 7/2^- [514] \otimes \pi 1/2^- [541]$ with a K value (4^+), which is less than the bandhead spin (5^+) on account of the aligned $1/2^- [541]$ proton that is involved. The initial alignment value of $4 \hbar$ (see Figure 4) supports the presence of this orbital.

In ref. [12], bands 2 and 3 were assigned different configurations, with $K^\pi = 3^+$ and $K^\pi = 4^+$ respectively, but this was largely due to incomplete experimental information. It is further noted that for band 2 there is a corresponding structure in ^{178}Ta , which was assigned $K^\pi=4^+$ [20], with $|g_K - g_R| = 0.18 \pm 0.02$. This compares well with the ^{180}Re value of 0.14 ± 0.02 .

The lowest level identified in band 2 forms the effective ground state of the high-spin part of the ^{180}Re level structure, as elaborated in the present work. There is no connection found with the level structure determined from β decay [6–9]. Furthermore, the assigned 5^+ member of the band is not necessarily the bandhead, as there could be an additional transition from the 5^+ state with a low energy (~ 30 keV) to which the present experiment is insensitive. Nevertheless, this would have no direct impact on the other spin, parity and configuration assignments discussed in this work, which use bands 4 and 11 as their basis.

4. Band 1, $K^\pi=(5^-)$, based on the 178 keV level

Two linked sequences of γ -ray transitions, corresponding to the present band 1, were previously identified [11] up to the 582 keV ($16 \rightarrow 14$) and 748 keV ($21 \rightarrow 19$) transitions. The bandhead de-excitation, however, was not established. In ref. [11], this band was assigned to ^{180}Re on the basis that it could not be associated with either of the neighboring isotopes ^{181}Re [24] and ^{179}Re [25], although the strongest transitions from this band were unresolved from γ rays emitted from both isotopes. In the present work, band 1 is confirmed

as belonging to ^{180}Re on the basis of coincidences observed with the 45.8 keV transition in band 2, and the lowest member of band 1 decays to band 2 through a tentatively identified 132.0 keV transition. This transition was observed in prompt coincidence with the strong transitions in band 1, see Figure 7. However, with five transitions assigned to ^{180}Re in the energy range 132.0-134.5 (see Table I) a firm placement of the 132.0 keV transition has not been possible. (Figure 7 also shows the presence of a 324.1 keV transition which was reported in ref. [11], and is still unplaced in the present level scheme.)

It remains problematical to determine the spin for the lowest level, at 178 keV, identified in band 1, because it might not be the bandhead, i.e. there could be additional unobserved transitions that are at low energy and highly converted. In this circumstance, transition intensity balancing cannot be used to determine the multipolarity of the 132 keV transition. Nevertheless, a spin change of one unit is implied, giving band 1 spins that are consistent with those of Venkova et al. [11]. However, we note that the systematics discussed more recently by Venkova et al. [26] favor assignments that are one spin unit higher. This could be made consistent with the present work by the insertion of a low-energy (unobserved) in-band transition at the bottom of the band, which would require the whole band to be shifted up by that transition energy.

Band 1 in ref. [11] was given a $\nu i_{\frac{13}{2}} \otimes \pi h_{\frac{9}{2}}$ assignment, i.e. $\nu 9/2^+[624] \otimes \pi 1/2^-[541]$. These two nucleons can couple to $K^\pi=4^-$ or 5^- , the former being energetically favored by the Gallagher-Moszkowski rules [27], although both nucleons are strongly affected by Coriolis mixing. Figure 4 shows that the alignment of this band is the largest of the 2-quasiparticle bands in ^{180}Re , about $5 \hbar$ at $\hbar\omega \approx 0.1$ MeV. Due to the strong Coriolis mixing, the K value is not well defined. However, the label $K^\pi=(5^-)$ is adopted since the simple g -factor analysis favors this value (see Table III). The K value is less than the apparent bandhead spin of 7^- , a feature that may be associated in particular with the $h_{\frac{9}{2}}, 1/2^-[541]$ proton, as with band 2.

B. Four-quasiparticle Bands

Four rotational bands (numbers 5, 6, 7 and 8) built on 4-quasiparticle intrinsic states have been observed in ^{180}Re . These bands were also reported in ref. [11], but, with the exception of band 8, they were not extended to high spin, and there are differences in the

bandhead decays. Due also to the reassignments of bands 4 and 11 (discussed above) new spin, parity and configuration assignments for the 4-quasiparticle bands are proposed in the present work. The four bands decay mainly via the 13^+ isomeric level at 1566 keV, the bandhead of band 5, into both bands 4 and 11. In optimising the statistical accuracy for the 13^+ bandhead lifetime, double energy gates were set (see Figure 8) on γ -ray transitions below the 13^+ bandhead and above the 16^+ , 1876 keV bandhead. It was found that, in addition to the 107 ± 2 ns mean-life for the 13^+ bandhead (see next section) it was necessary to include an additional component with a mean-life of 7 ± 1 ns. However, it was not possible to determine to which one or more of the three intermediate bandheads (14^- , 15^- or 16^+) this should be ascribed. Accordingly, we consider that each intermediate bandhead has $\tau < 8$ ns.

1. *Band 5, $K^\pi=13^+$, based on the 1566 keV level*

Band 5 has an isomeric bandhead with a mean-life of 107 ± 2 ns (see Figure 8). The isomer was previously identified in both refs. [10, 11], with consistent lifetimes, though the present measurement has a smaller uncertainty. The multiplicities of some of the isomeric transitions are listed in Table II. The conversion coefficient of the 678.1 keV transition is measured to be $\alpha_K=0.008(1)$, which establishes its E2 character and leads to the $I^\pi = K^\pi = 13^+$ assignment for the isomer. At least four quasiparticles are needed to provide such a high K value, and the excitation energy of 1566 keV is consistent with the energy required to break one additional nucleon pair relative to the 2-quasiparticle states. The associated rotational sequence (band 5) is very weakly populated and is tentatively placed in the level scheme (Figure 2).

Band 5 is suggested to have the configuration $\nu 7/2^- [514], 9/2^+ [624], 5/2^- [512] \otimes \pi 5/2^+ [402]$. The alignment value (Figure 4) $i_x = 3.5\hbar$ at $\hbar\omega \approx 0.15$ MeV, is consistent with the involvement of a single $i_{\frac{13}{2}}$ neutron. This relatively low alignment and non-yrast location, compared to the higher-K 4-quasiparticle bands, can explain its weak population.

2. *Band 6, $K^\pi=14^-$, based on the 1700 keV level*

Band 6 decays by a 134.1 keV transition to the 13^+ bandhead, and by an 895.3 keV transition to the 12^- state of band 11. The total conversion coefficient for the 134.1 keV transition indicates E1 character [11], hence $I^\pi=14^-$ for the bandhead. The band is assigned the configuration $\nu 7/2^- [514], 9/2^+ [624], 7/2^+ [633] \otimes \pi 5/2^+ [402]$. The alignment of $i_x = 5.5\hbar$ at $\hbar\omega \approx 0.15$ MeV (Figure 4) is consistent with the involvement of two $i_{\frac{13}{2}}$ neutrons.

3. *Band 7, $K^\pi=15^-$, based on the 1755 keV level*

The assignment of $K^\pi=15^-$ to band 7 is based on the new placement of the 54.8 keV transition, which was reported in ref. [11] and tentatively identified as coming from an isolated isomeric level, though the lifetime was not measured and the band associated with it was not seen. It is now established that band 7 is associated with the 54.8 keV transition (see Figure 9). It was not possible to establish a lifetime associated specifically with the 54.8 keV transition but an upper limit of $\tau < 8$ ns can be set. The isomeric nature previously attributed to the corresponding level in ref. [11] is understood to be due to a higher-lying long-lived isomer (see later for more details). From intensity balancing, the 54.8 keV transition has $\alpha_{TOT}=7\pm 2$ which strongly suggests M1 ($\alpha_{TOT}=5.4$) rather than E2 ($\alpha_{TOT}=59.4$) or E1 ($\alpha_{TOT}=0.38$) character, thereby establishing a bandhead spin of 15^- .

The proposed configuration is $\nu 7/2^- [514], 9/2^+ [624], 5/2^- [512] \otimes \pi 9/2^- [514]$. Another $K^\pi=15^-$ state is also possible, from the $\nu 7/2^- [514], 9/2^+ [624], 7/2^+ [633] \otimes \pi 7/2^+ [404]$ configuration. In this case the relatively small alignment of $i_x = 4\hbar$ at $\hbar\omega \approx 0.15$ MeV favors the former configuration, involving a single $i_{\frac{13}{2}}$ neutron. The relatively low alignment is consistent also with the weak population of the band. A comparable $K^\pi=15^-$ band has also been observed in ^{178}Ta [20] with a similar $|g_K - g_R| = 0.16 \pm 0.02$ (compared with 0.18 ± 0.09 for ^{180}Re). A different configuration mixing was discussed in that case, though with the same dominant structure.

It is also notable that band 7 is crossed by band 6, and the unfavored members of band 7 are not identified above the crossing. Further discussion of the crossing is given in Section IV. This interpretation provides additional evidence in support of the proposed level structure and the relative spin and parity assignments. Indeed, in our preliminary report [13] bands

6 and 7 were swapped (relative to what is now presented) but the identification of the 319 keV γ -ray as an interband transition now removes the ambiguity.

4. *Band 8, $K^\pi=16^+$, based on the 1876 keV level*

Band 8 decays to the 15^- bandhead by a 120.5 keV transition with $\alpha_{TOT}=0.6\pm 0.3$ (see Table II) which implies an E1 assignment ($\alpha_{TOT}=0.24$) hence $I^\pi=16^+$ for the bandhead of band 8. A configuration assignment of $\nu 7/2^- [514], 9/2^+ [624], 7/2^+ [633] \otimes \pi 9/2^- [514]$ is suggested. The presence of two $i_{13/2}$ neutrons is consistent with the high initial bandhead alignment of $i_x = 5.5\hbar$ at $\hbar\omega \approx 0.15$ MeV (see Figure 4). The adopted configuration is the same as for the $K^\pi=16^+$ band in ^{178}Ta , which has $|g_K - g_R| = 0.10 \pm 0.01$ [20], compared to the ^{180}Re value of 0.16 ± 0.03 .

The structure of band 8 is related to that of band 4 with the addition of a neutron $(i_{13/2})^2$ excitation, where the $9/2^+ [624]$ and $7/2^+ [633]$ neutrons are coupled to $K \approx 8$. This is the so-called t -band structure, which was first identified in ^{179}W [19], an isotone of ^{180}Re . While in ^{179}W the 3-quasiparticle t -band crosses its respective 1-quasiparticle g -band, in ^{180}Re the 4-quasiparticle, $K^\pi=16^+$ t -band is already energetically favored compared to its corresponding 2-quasiparticle, $K^\pi=8^+$ “ g -band”, so that no crossing can take place. In principle, given sufficient interaction between these two bands, a 164-keV, E2 transition might be observable from the $K^\pi=16^+$ bandhead to the 14^+ member of the $K^\pi=8^+$ band, but this has not been identified in the present work. A remarkably similar situation exists in ^{178}Ta [20], where the corresponding E2 interband transition would have an energy of 190 keV.

The energy differences between the t - and g -bands in the $N=105$ isotones ^{178}Ta and ^{180}Re , compared to ^{179}W , can be understood to arise from two factors. First, due to the higher spins in the odd-odd isotones from the additional quasiparticle, the rotational energies are greater, favoring the $\Delta K \approx 8$, t -band excitation. Second, the residual interactions with the odd proton give additional favoring to the t -band configuration. Hence, it may be concluded, the $g-t$ bandcrossing observed in ^{179}W is absent in ^{178}Ta and ^{180}Re , because the respective t -bands are already energetically favored at their bandheads.

C. Six-quasiparticle Bands

Two new bands, numbers 9 and 10, are assigned to ^{180}Re . These are associated with a high-lying isomer for which initial evidence was reported in ref. [11]. A mean-life of 13 ± 1 μs has now been measured, as illustrated in Figure 10. The principal decay path of the isomer is by a 456.8 keV transition (see Figure 9) to band 8. The isomer decays through two other routes. One is to a state at 3408.4 keV via an unobserved 62.9 keV transition. (This transition could not be separated from the intense 61.1 keV $K_{\alpha 1}$ X-rays of ^{180}Re .) The other decay route is via a 102.2 keV transition, illustrated in Figure 11, to a state at 3369.1 keV which decays in turn via an 1164.1 keV transition to the $I^\pi=17^-$ member of band 11.

1. Band 9, $K^\pi=21^-$, based on the 3471 keV level

Band 9 is built on the 13 μs isomeric state and decays to the 20^+ state of band 8 via a 456.8 keV transition (see Figure 9) which is found to be of E1 character from its directly measured conversion coefficient of $\alpha_K = 0.0084 \pm 0.0010$. Deduction of this conversion coefficient was complicated by the fact that ^{177}Ta [28], which was significantly populated, has a 456.7 keV transition below an isomeric level of comparable mean-life (8.6 ± 0.3 μs) to that of the 456.8 keV transition in ^{180}Re . However, the K binding energy differences result in conversion lines which are partially resolved, hence component electron intensities can be obtained, see Figure 12. The corresponding γ -ray intensities can be determined with the aid of γ - γ -coincidences. With implied E1 character for the 456.8 keV transition, the bandhead of band 9 is assigned $I^\pi=K^\pi=21^-$.

Multi-quasiparticle calculations (see Section IV) indicate that there are two competing configurations, with the required spin and parity, which could be assigned to the 21^- state at 3471 keV:

$$\begin{aligned} & \nu 9/2^+[624] \otimes \pi 5/2^+[402], 9/2^-[514], 7/2^+[404], 1/2^-[541], 11/2^-[505]; \text{ and} \\ & \nu 7/2^-[514], 9/2^+[624], 5/2^-[512] \otimes \pi 5/2^+[402], 9/2^-[514], 7/2^+[404]. \end{aligned}$$

The second of these involves only one aligning quasiparticle and is favored by the relatively low alignment of the band, $i_x = 5\hbar$ at $\hbar\omega \approx 0.15$ MeV, as seen in Figure 4. The weak population of the band is also consistent with its low alignment.

2. *Band 10, $K^\pi=(22^+)$, based on the 3895 keV level*

Band 10 feeds into the 13 ± 1 μs isomer via a 424.0 keV transition (see Figure 13). In the absence of a significant lifetime, the 424 keV transition is tentatively assigned dipole character, and the bandhead of band 10 is assigned $I=(22)$. Consequently, there is a crossing between bands 9 and 10 at $I=25$, with close-lying states of equal spin. The lack of interband transitions or significantly perturbed energy levels suggests that the two bands have opposite parities, hence band 10 is tentatively assigned positive parity.

Multi-quasiparticle calculations predict a low-lying 22^+ state with the configuration $\nu 7/2^- [514], 7/2^+ [633], 9/2^+ [624] \otimes \pi 5/2^+ [402], 9/2^- [514], 7/2^+ [404]$. The involvement of two $i_{13/2}$ neutrons gives extra alignment compared to band 9 and is consistent with the observed value of $i_x = 6\hbar$ at $\hbar\omega \approx 0.15$ MeV (see Figure 4). This leads to the crossing with band 9, despite band 10 being unfavored at its bandhead, and it furthermore explains the relatively strong population of band 10. Indeed, band 10 extends to the highest spin, $I=(29)$, identified in ^{180}Re .

A similar band has been found in ^{178}Ta [20] with the same configuration assignment. As with the other corresponding bands in these two isotones, the alignment in the ^{180}Re band is about $2\hbar$ higher than in the ^{178}Ta band. However, the g -factors seem to differ significantly. The ^{178}Ta band has $|g_K - g_R| = 0.25 \pm 0.04$, compared to 0.12 ± 0.06 for the ^{180}Re band. The latter value has a large percentage uncertainty arising from the band's weak population, and improved accuracy would clearly be needed for a more discriminating comparison.

D. Other States

The ability to measure γ - γ coincidences *in between* beam pulses gives great sensitivity to transitions that follow isomeric decays. Combined with the high spin, $I=21$, of the 6-quasiparticle isomer in ^{180}Re , the method enables several non-yrast high-spin states to be identified, as illustrated Figure 2. In the absence of rotational bands associated with these states, the possible configuration assignments cannot be reliably determined.

The 62.9 keV transition from the 21^- bandhead (band 9) and the 84.5 keV transition from the 15^- bandhead (band 7) are not themselves observed, but their existence is required by the γ -ray coincidence relationships. The spins and parities of the various states are determined

through their connections to the bands already discussed, by intensity flow considerations with corresponding conversion-coefficient constraints, and by directly measured conversion coefficients.

IV. DISCUSSION

The level scheme for ^{180}Re is discussed in a selective way in the following sections. After an analysis of the low-spin bandcrossing, bandhead excitation energies are compared with multi-quasiparticle calculations, and finally the hindrances of the K-forbidden decays are examined.

A. Bandcrossings

It has been established that there are several γ -ray transitions between bands 2 and 3, indicating an interaction between the two bands. Figure 14 depicts the crossing in a plot of excitation energy versus spin, including also the other 2-quasiparticle bands. The interaction matrix element, V , is evaluated with the usual two-band-mixing approach (see, for example, ref. [21]) making use of the in-band/out-of-band $B(E2)$ ratios. The intrinsic (unperturbed) transition matrix elements are taken from the rotational model. The interaction has been calculated for two cases, see Table IV, first with equal K for both bands, and second with different K values. It is clear that the different- K assumption gives better consistency for the calculated interaction strengths, with an average value of $V=7.3\pm 0.4$ keV. This is in accord with the assigned K values discussed earlier. Figure 15 illustrates the level energy differences $\Delta E(I \rightarrow I-1)/2I$ versus spin, showing both the perturbed (experimental) values and the unperturbed values (with the interaction removed). This representation is sensitive, in the form of odd-even staggering, to interactions between bands. It is seen that a constant interaction matrix element of $V=7.3$ keV produces smooth curves for the unperturbed bands in the $I=11$ crossing region. This analysis thus provides a good description of the crossing between bands 2 and 3, including the interband transition strengths, and gives support to the validity of the relative spin and parity assignments.

There is another bandcrossing. Band 6 crosses band 7, but the continuation of band 7 is not observed. Mixing is indicated by the presence of the 319.2 keV transition from the

TABLE IV: Mixing matrix elements between bands 2 and 3 in ^{180}Re .

I_i^π	E_γ (keV)	I_γ	V (keV) ^{a)}	V (keV) ^{b)}
13^+	416.4	54(11)	– ^{c)}	– ^{c)}
	435.6	102(23)		
13^+	508.3	8(2)	7.23(5)	7.71(5)
	489.2	55(10)		
12^+	410.6	45(20)	6.59(12)	7.34(12)
	382.4	174(36)		
11^+	383.7	86(15)	9.08(14)	6.91(14)
	333.3	65(15)		
11^+	352.5	11(3)	4.90(12)	7.59(12)
	403.4	38(7)		

^{a)} Calculated with equal K for both bands.

^{b)} Calculated with K=7 for band 3 and K=4 for band 2.

^{c)} No solution found.

$I^\pi=19^-$ member of band 6 to the $I^\pi=18^-$ member of band 7 (see Figure 2). Figure 16 shows the energy-versus-spin diagram for the 4- and 6-quasiparticle bands in ^{180}Re , including bands 6 and 7, for which the approach to bandcrossing is evident. However, the weak population of bands 6 and 7, and the non-observation of the unfavored states above the crossing, make the mixing strength difficult to quantify.

B. Nilsson-plus-BCS calculations

The proposed quasiparticle configurations for the bands in ^{180}Re have been calculated using two separate methods. The first method, discussed in this section, is that of K. Jain et al. [32], based on the Nilsson model and BCS pairing with blocking by quasiparticle excitations. A full set of near-yrast multi-quasiparticle states was calculated. In this process, empirical single-particle energies were used for states close to the Fermi surface, estimated from 1-quasiparticle energies, where available, in neighboring odd-mass nuclei (^{179}Re , ^{181}Re

for protons, and ^{179}W , ^{181}Os for neutrons [33]). In order to produce the correct average particle number the Fermi level was recalculated for each configuration. The monopole pairing force was $G_\nu = \frac{21.5}{A} = 0.119$ MeV for neutrons and $G_\pi = \frac{22.5}{A} = 0.125$ MeV for protons, and the deformation parameters were $\epsilon_2 = 0.232$ and $\epsilon_4 = 0.047$ [31]. The proton and neutron levels were treated separately to create their multi-quasiparticle states, and then the two were combined. Residual interactions were also taken into account, using the empirical 2-quasiparticle Gallagher-Moszkowski splittings [27, 34] according to the method of K. Jain et al. [32]. The resultant multi-quasiparticle energies can then be compared with the experimental values.

Generally good agreement is found between theoretical and experimental 2-, 4- and 6-quasiparticle energies as seen in Table V (compare the columns ‘‘Calc.III’’ and ‘‘Expt.’’) with the notable exception of the $K^\pi=21^-$ state. The energy calculated for this level (residual interactions included) is higher than the experimental energy by 378 keV. (In the case of ^{178}Ta , the corresponding calculated energy, with Lipkin-Nogami pairing, was in good agreement [20].) The reason for the discrepancy in ^{180}Re may be partly due to the simple BCS treatment of pairing, and partly due to the fixed-deformation constraint in the calculations. There is a significant discrepancy (>200 keV) also for the 2-quasiparticle $K^\pi=5^-$ bandhead. Both of these cases are predicted (see next section) to have large quadrupole deformations. The $K^\pi=5^-$ configuration could be a special case due to large Coriolis mixing and the proximity of the favored $K^\pi=4^-$ coupling (see also Section III). The configurations are summarised in Table III.

A graphical comparison between calculated and experimental energies is given in Figure 17, including additional low-lying multi-quasiparticle states. The following observations can be made:

- (i) Calculated $K^\pi = 13^-$ and 12^- states have reasonable correspondence with the experimental states at 1670 and 1403 keV, respectively (see Figure 2). These both have the configuration $\nu 7/2^- [514], 9/2^+ [624], 1/2^- [521] \otimes \pi 9/2^- [514]$, with maximal $K=13$ in one case, and $K=12$ from the opposed orientation of the $1/2^- [521]$ neutron in the other.
- (ii) Additional calculated states with $K^\pi = 14^+$ and 15^- are illustrated, with no corresponding experimental states. These predictions appear to be reasonable, in that their higher excitation energies are consistent with their non-observation experimentally.
- (iii) A $K^\pi = 19^-$ state is calculated at 2704 keV, with the configuration

$\nu 7/2^- [514], 9/2^+ [624], 7/2^+ [633] \otimes \pi 9/2^- [514], 5/2^+ [402], 1/2^- [541]$. This might possibly correspond to the higher-energy experimental level at 3369 keV (see also next section).

C. Potential Energy Surface Calculations

Potential-energy-surface (PES) calculations using the configuration-constrained method of Xu et al. [35] have been used as a second approach for understanding the multi-quasiparticle states. In this approach, the Woods-Saxon potential (with no adjustment of single-particle energies) and Lipkin-Nogami pairing were used. For each quasiparticle configuration, the occupied orbitals were fixed and the quadrupole and hexadecapole deformations, β_2 , γ and β_4 , were varied in order to minimise the excitation energy. (Note that $\epsilon_2 \approx 0.94\beta_2$.) The neutron and proton monopole pairing strengths were determined by the average gap method [36] with a 10% enhancement [35]. Due to the additional complexity of this method, only selected ^{180}Re multi-quasiparticle states were calculated, with results given in Tables III and V. The calculated excitation energies agree satisfactorily with the experimental results, and are broadly consistent with the Nilsson-plus-BCS calculations. The variable-shape PES method gives substantially better agreement for the experimental $K^\pi = 5^-$ and 21^- energies, with large calculated β_2 values. Furthermore, the $K^\pi = 19^-$ state that has a low energy of 2704 keV from the Nilsson-plus-BCS calculations (discussed above) has also been calculated with the PES method. It is predicted to lie at 3340 keV, which is close in energy to the observed (19^-) level at 3369 keV.

Overall, the combination of a more realistic potential, a better treatment of pairing, and variable shape, combine to make the PES calculations more reliable than the Nilsson-plus-BCS calculations.

D. K-Forbidden Transitions

The projection, K , of the total angular momentum on the symmetry axis is approximately a good quantum number for deformed axially symmetric nuclei. This defines the K -selection rule for electromagnetic transitions, $\Delta K \leq l$, for multipolarity l . In practice, transitions which violate this selection rule are hindered rather than forbidden, due to K -mixing mechanisms. A measure of the inhibition can be expressed by the hindrance factor, $F_W = \tau^\gamma / \tau^W$,

TABLE V: Properties of ^{180}Re bandheads (see also Table III).

Band	K^π	Deformations ^{a)}			Energy (keV)			
		β_2	β_4	$ \gamma^\circ $	Calc.I ^{a)}	Calc.II ^{b)}	Calc.III ^{c)}	Expt. ^{d)}
1	5^-	0.246	-0.031	0.0	270	468	503	178
2	4^+	0.215	-0.030	0.0	60	253	178	0
3	7^+	0.224	-0.044	0.2	60	214	111	71
4	8^+	0.240	-0.034	0.6	80	167	217	205
11	9^-	0.224	-0.033	0.2	190	382	311	284
5	13^+	0.242	-0.040	0.2	1560	1697	1558	1566
6	14^-	0.229	-0.043	0.0	1600	1661	1567	1700
7	15^-	0.239	-0.030	0.2	1670	1864	1722	1755
8	16^+	0.224	-0.033	0.3	1710	1829	1751	1876
9	21^-	0.247	-0.025	0.1	3350	4187	3849	3471
10	22^+	0.267	-0.027	0.2	3740	4152	3890	3895

^{a)} PES calculations using the method of Xu et al. [35].

^{b)} Fixed-shape calculations ($\beta_2 \approx 0.25$) using the method of K. Jain et al. [32] without residual interactions.

^{c)} Fixed-shape calculations including residual interactions [34].

^{d)} Experimental energies are given relative to the bandhead of band 2 ($K^\pi = 4^+$).

which is the ratio of the partial γ -ray mean-life to the Weisskopf single-particle estimate [37]. The hindrance per degree of K forbiddenness, also call the reduced hindrance, is $f_\nu = F_W^{1/\nu}$, where $\nu = \Delta K - l$ is the degree of forbiddenness. In refs [37, 38] it was found that $f_\nu \approx 100$ for a range of ν and l , so that for each additional unit of ΔK , transitions are hindered by an additional factor of about 100. This situation is well illustrated [39] by the decay of high-K isomers in ^{178}Hf , which is arguably located at the center of the K-isomer region [2]. However, many transitions have also been found in the same region with $f_\nu \ll 100$, see for example refs [19, 40–45], giving valuable information about the way that K mixing takes place. Since ^{180}Re is on the high-Z side of this K-isomer region, the reduced hindrance values may shed further light on the K-mixing mechanisms.

One transition of particular note with regard to K-forbidden transitions is the 1164 keV,

(19^-) to 17^- transition from the 3369 keV level. Although of low intensity it is well established, as demonstrated in Figure 11. Considering, tentatively, the (19^-) level as an intrinsic state with $K^\pi=19^-$, the 1164 keV transition would have E2 character and change the K value by 10 units, i.e. it would be highly K forbidden, with $\nu=8$, bypassing the intermediate-K structures. Due to the low population intensity and the feeding through the 13 μ s isomer, the lifetime of the 3369 keV level has a relatively poor constraint of $\tau < 100$ ns, obtained from the observed coincidence between the 1164 keV transition and the 102 keV feeding transition. Nevertheless, this limit indicates a significantly small reduced hindrance value, $f_\nu < 4.4$. Such a low value may be related to the location of the (19^-) level relatively far from the yrast line, which is broadly consistent with the systematic behavior discussed by Walker et al. [2, 46].

More definite information can be obtained for K-forbidden transitions with known (partial) half-lives. Table VI lists the transitions in ^{180}Re from the 4- and 6-quasiparticle isomers with $K^\pi=13^+$ and 21^- , respectively. Note that for E1 transitions two values are given, the second with τ^W multiplied by 10^4 before recalculating f_ν , to account for the generally strong E1 hindrance compared with other multiplicities [47, 48]. The final reduced-hindrance values vary between 17 and 66.

The E2 reduced-hindrance value for the 678 keV transition from the $K^\pi=13^+$ isomer, $f_\nu = 17$, may now be compared with systematic behavior in the $A \approx 180$ region. In previous work, K-forbidden E2 and E3 reduced hindrances from 4- and 5-quasiparticle isomers have been compared, through their inverse correlation with excitation energy relative to a rigid rotor, indicating a level-density dependence in the degree of K mixing [2, 46, 49]. The data are shown in Figure 18, with the odd-odd nuclides [20, 50–52] specifically indicated. It has been suggested [53] that the large reduced hindrance for ^{178}Ta may be related to neutron-proton configuration mixing. In any case, the ^{180}Re value is in relatively good agreement with the trend of the other data. This supports the proposition that level density plays a critical role in K mixing, though the sizeable scatter of the data also indicates the importance of other degrees of freedom [2].

In Figure 19, the yrast line is compared with the excitation energies of intrinsic states. Following from the above discussion, states which lie well above the yrast line are expected to have more K admixtures than the near-yrast states, and hence lower f_ν values. In ^{180}Re , both the $K^\pi = 13^+$ and 21^- isomers are not too far from yrast and the f_ν values are

TABLE VI: K-forbidden transitions in ^{180}Re .

K_i^π	τ	E_γ (keV)	l	I_γ ^{a)}	α_{TOT}	$B(\sigma l)$ ($e^2 fm^{2l}$ for El) ($\mu_o^2 fm^{2l-2}$ for Ml)	ν	f_ν ^{b)}	
21^-	13(1) μs	62.9	E1	53(18) ^{c)}	0.260	$3.6(15) \times 10^{-8}$			
		102.2	E2	21(10)	3.84	$4.2(25) \times 10^{-3}$			
		456.8	E1	118(10)	0.009	$2.1(6) \times 10^{-10}$	4	315(19)	31.5(19)
13^+	107(2) ns	141.4	M1	38(10)	2.01	$2.0(6) \times 10^{-5}$	4	20.5(14)	
		163.1	E1	60(8)	0.109	$1.15(17) \times 10^{-6}$			
		262.4	E1	38(7)	0.033	$1.7(4) \times 10^{-8}$	3	490(40)	22.7(15)
		416.6	M1	198(15)	0.103	$2.1(2) \times 10^{-6}$	4	30.5(8)	
		523.5	E1	60(9)	0.007	$3.5(6) \times 10^{-9}$	3	840(50)	38.9(22)
		678.1	E2	169(23)	0.011	$1.3(2) \times 10^{-2}$	3	16.8(9)	
		761.0	E1	38(5)	0.003	$7.1(11) \times 10^{-10}$	3	1420(70)	66(4)

^{a)}From Table I.

^{b)}Including an additional factor of 10^4 in hindrance before the evaluation of f_ν

^{c)}From 285.7 keV transition intensity.

substantial.

It is notable that ^{180}Re is the only odd-odd rhenium isotope known to display K isomerism for a 6-quasiparticle state. Neighboring ^{179}Re has recently been found to contain a 7-quasiparticle isomer [4]. While this also decays by transitions with substantial f_ν values, uncertainty in the isomer spin assignment makes the interpretation ambiguous in that case.

V. SUMMARY

In the present work, eleven rotational bands in ^{180}Re have been observed and characterised by γ -ray and electron spectroscopy. The bands have been extended to higher spin compared to previous studies. Amongst the 2-quasiparticle bands, new connecting transitions have enabled significant improvements to be made in the organisation of the level scheme, leading to revised spin and parity assignments, and hence to a revised interpretation. This builds

on the theoretical analysis of the 2-quasiparticle bands by Jain et al. [12].

The present work provides a new and detailed bandcrossing analysis of 2-quasiparticle bands 2 and 3. The properties of a 4-quasiparticle t -band are compared with related structures in the $N=105$ isotones. Two bands are identified above a 6-quasiparticle, $\tau=13 \mu\text{s}$ isomer. Configuration assignments are given for all the bands, supported by multi-quasiparticle calculations, alignments and g -factors.

The 4- and 6-quasiparticle isomers in ^{180}Re are found to decay by K-forbidden transitions. The substantial reduced-hindrance values, $17 \leq f_{\nu} \leq 66$, are most likely related to the near-yrast location of the isomers.

Acknowledgements: The ANU technical staff are thanked for their excellent support. This work has been performed under an ANU–EPSRC agreement. JNO and AE were funded by EPSRC project studentships.

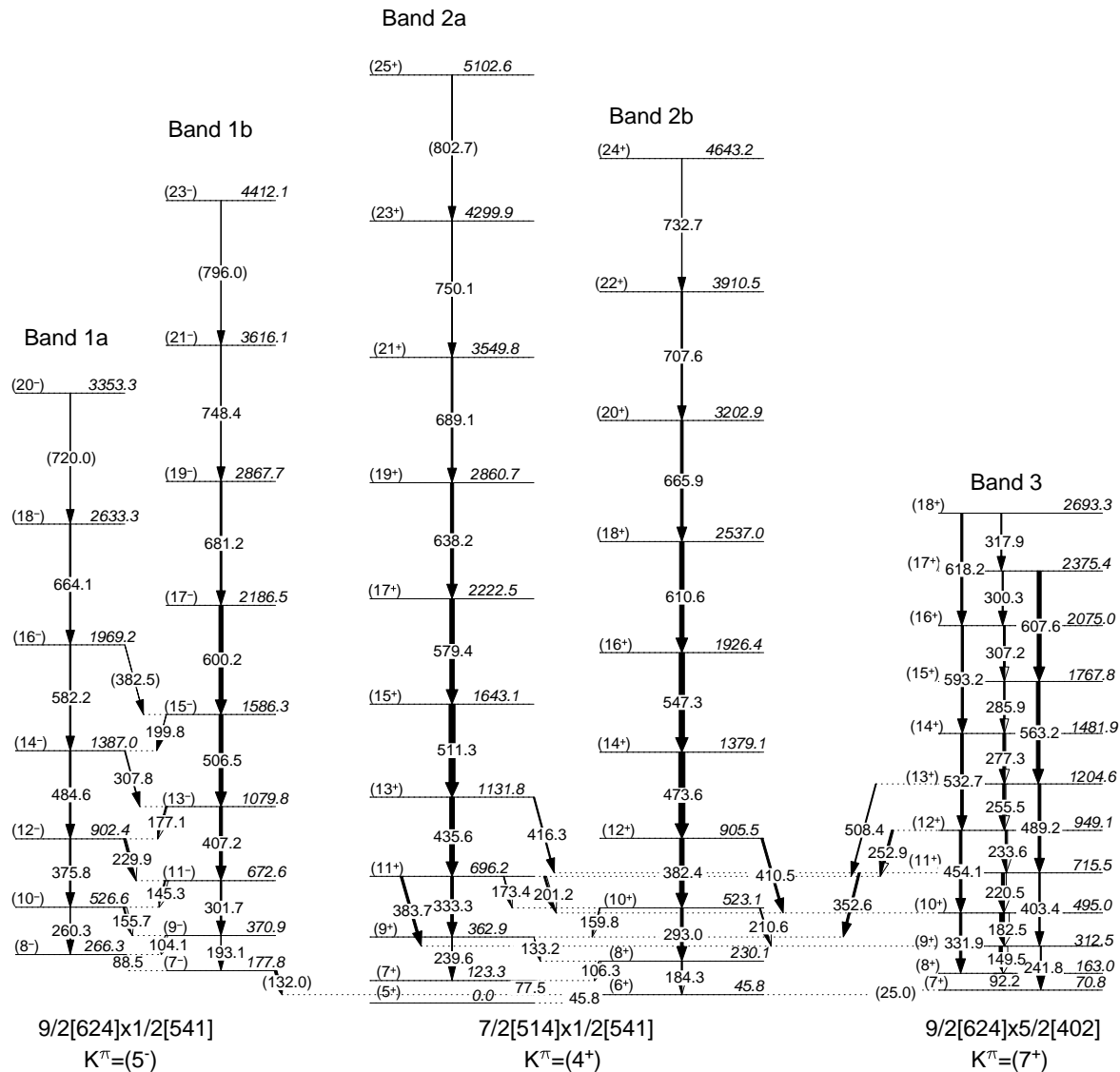
-
- [1] M.J.A. de Voigt, J. Dudek, and Z. Szymanski, *Rev. Mod. Phys.* **55**, 949 (1983).
 - [2] P.M. Walker, and G.D. Dracoulis, *Hyperfine Interact.* **135**, 83 (2001).
 - [3] R.G. Helmer, and C.W. Reich, *Nucl. Phys.* **A211**, 1 (1973).
 - [4] C. Thwaites, C. Wheldon, A.M. Bruce, P.M. Walker, G.D. Dracoulis, A.P. Byrne, T. Kibédi, F.G. Kondev, C.J. Pearson and C.S. Purry, *Phys. Rev. C* **66**, 054309 (2002).
 - [5] C.J. Pearson, P.M. Walker, C.S. Purry, G.D. Dracoulis, S. Bayer, A.P. Byrne, T. Kibédi, and F.G. Kondev, *Nucl. Phys.* **A674**, 301 (2000).
 - [6] K.J. Hofstetter, and P.J. Daly, *Phys. Rev.* **152**, 1050 (1966); *ibid* **159**, 1000 (1967).
 - [7] P.F.A. Goudsmit, J. Konijn, and F.W.N. de Boer, *Nucl. Phys.* **A104**, 497 (1967).
 - [8] B. Harmatz, and T. H. Handley, *Nucl. Phys.* **A121**, 481 (1968).
 - [9] J. Konijn, P.F.A. Goudsmit, F.W.N. De Boer, and B.J. Meijer, *Nucl. Phys.* **A114**, 602 (1968).
 - [10] A. J. Kreiner, J. Davidson, D. Abriola, C. Pomer, and P. Thieberger, *Phys. Rev.* **C37**, 1338 (1988).
 - [11] Ts. Venkova, R. M. Lieder, T. Morek, W. Gast, G. Hebbinghaus, A. Kramer-Flecken, J. Schaffler-Krah and W. Urban, *Nucl. Phys.* **A514**, 87 (1990).
 - [12] A.K. Jain, P.C. Sood, and R.K. Sheline, *Pramana J. Phys.* **43**, 339 (1994).
 - [13] H.M. El-Masri, P.M. Walker, Z. Podolyák, M. Caamaño, G.D. Dracoulis, A.P. Byrne,

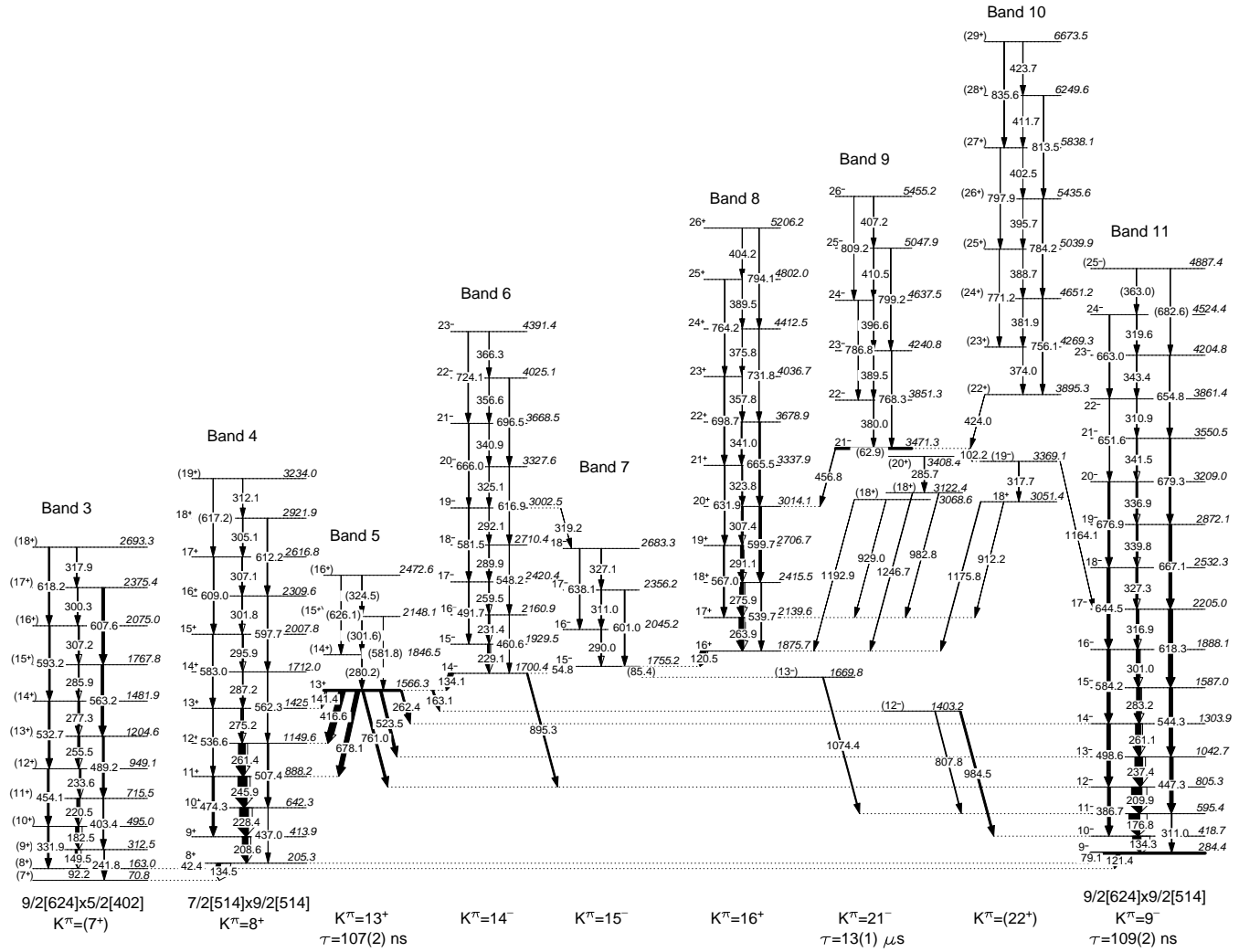
- T. Kibédi, A.M. Baxter, J. Hazel, A.M. Bruce, J.N. Orce, A. Emmanoulidis, D.M. Cullen, and C. Wheldon, *Acta Phys. Pol.* **B34**, 2301 (2003).
- [14] F. Puhlhofer, *Nucl. Phys.* **A280**, 267 (1977).
- [15] G.D. Dracoulis and A.P. Byrne, ANU-P/1052 (1995), unpublished.
- [16] T. Kibédi, G.D. Dracoulis, and A.P. Byrne, *Nuc. Instr. and Meth.* **A294**, 523 (1990).
- [17] A. Karamer-Flecken, T. Morek, R.M. Lieder, W. Gast, G. Hebbinghaus, H.M. Jager, and W. Urban, *Nuc. Instr. and Meth.* **A275**, 333 (1989).
- [18] F. Rösler, H.M. Fries, K. Alder, and H.C. Pauli, *At. Nucl. Data Table* **21**, 291 (1978).
- [19] P.M. Walker, G.D. Dracoulis, A.P. Byrne, B. Fabricius, T. Kibédi, A.E. Stuchbery, and N. Rowley, *Nucl. Phys.* **A568**, 397 (1994).
- [20] F.G. Kondev, G.D. Dracoulis, A.P. Byrne and T. Kibédi, *Nucl. Phys.* **A632**, 473 (1998).
- [21] C.S. Purry, P.M. Walker, G.D. Dracoulis, T. Kibédi, F.G. Kondev, S. Bayer, A.M. Bruce, A.P. Byrne, W. Gelletly, P.H. Regan, C. Thwaites, O. Burglin, and N. Rowley, *Nucl. Phys.* **A632**, 229 (1998); C.S. Purry, PhD thesis, University of Surrey, (1997).
- [22] R.A. Bark, G.B. Hagemann, B. Herskind, H.J. Jensen, W. Korten, J. Wrzesinski, H. Carlsson, M. Bergstrom, A. Brockstedt, A. Nordlund, H. Ryde, P. Bosetti, S. Leoni, F. Ingelbrechtsen, P.O. Tjom, *Nucl. Phys.* **A591**, 265 (1995).
- [23] T. Lindbland, H. Ryde, and P. Kleiheinz, *Nucl. Phys.* **A201**, 369 (1973).
- [24] A. Neskakasi, R.M. Reider, M. Muller-Veggian, H. Beuscher, W.F. Davidson, and C. Mayer-Boriche, *Nucl. Phys.* **A261**, 189 (1976).
- [25] Ts. Venkova, T. Morek, R.M. Lieder, W. Gast, G. Hebbinghaus, A. Krammer-Flecken, J. Schaffler-Krah, W. Urban, G. Sletten, and K.H. Maier, *Z. Phys.* **A334**, 385 (1989).
- [26] Ts. Venkova et al., *Eur. Phys. J.* **A20**, 375 (2004).
- [27] C.J. Gallagher, and S.A. Moskowsky, *Phys. Rev.* **111**, 1282 (1958).
- [28] M. Dasgupta, G.D. Dracoulis, P.M. Walker, A.P. Byrne, T. Kibédi, F.G. Kondev, G.J. Lane, and P.H. Regan, *Phys. Rev.* **C61**, 044321 (2000).
- [29] P.M. Walker, K.C. Yeung, G.D. Dracoulis, P.H. Regan, G.J. Lane, P.M. Davidson and A.E. Stuchbery, *Phys. Lett.* **B309**, 17 (1993).
- [30] P.M. Walker, *Proceedings of the Crete Conference on The Future Of Nuclear Spectroscopy*, edited by W. Gelletly, C.A. Kalfas, R. Vlastou, S. Harissopulos and D. Loukas, Institute of Nuclear Physics (Greece), 134 (1993).

- [31] R. Bengtsson, S. Frauendorf, and F.R. May, *At. Nucl. Data Tables* **35**, 15 (1986).
- [32] K. Jain, O. Burglin, G.D. Dracoulis, B. Fabricius, N. Rowley, and P.M. Walker, *Nucl. Phys.* **A591**, 61 (1995).
- [33] R.B. Firestone, and V.S. Shirley (Eds.), *Table of Isotopes*, 8th edition (Wiley, 1996).
- [34] F.G. Kondev, PhD thesis, Australian National University, (1996).
- [35] F.R. Xu, P.M. Walker, J.A. Sheikh and R. Wyss, *Phys. Lett.* **B435**, 257 (1998).
- [36] P. Möller, J.R. Nix, *Nucl. Phys.* **A536**, 120 (1992).
- [37] K.E.G. Löbner, in *The electromagnetic interaction in nuclear spectroscopy*, W.D. Hamilton (Ed.) (North-Holland, Amsterdam, 1975) p. 141.
- [38] K.E.G. Löbner, *Phys. Lett.* **B26**, 369 (1968).
- [39] M.B. Smith, P.M. Walker, G.C. Ball, J.J. Carroll, P.E. Garrett, G. Hackman, R. Propri, F. Sarazin, and H.C. Scraggs, *Phys. Rev.* **C68**, 031302(R) (2003).
- [40] P. Chowdhury, B. Fabricius, C. Christensen, F.Azgui, S.Bjornholm, J. Borggreen, A. Holm, J.Pedersen, G. Sletten, M.A. Bentley, D. Howe, A.R. Mokhtar, J.D. Morrison, J.F. Sharpey-Schafer, P.M. Walker, and R.M. Lieder, *Nucl. Phys.* **A485**, 136 (1988).
- [41] P.M. Walker, G. Sletten, N.L. Gjørup, M.A. Bentley, J. Borggreen, B. Fabricius, A. Holm, D. Howe, J. Pedersen, J.W. Roberts, and J. F. Sharpey-Schafer, *Phys. Rev. Lett.* **65**, 416 (1990).
- [42] N.L. Gjørup, P.M. Walker, G. Sletten, M.A. Bentley, B. Fabricius, and J.F. Sharpey-Schafer, *Nucl. Phys.* **A582**, 369 (1995).
- [43] P.M. Walker, G.D. Dracoulis, A.P. Byrne, B. Fabricius, T. Kibédi, and A.E. Stuchbery, *Phys. Rev. Lett.* **67**, 433 (1991).
- [44] B. Crowell, P. Chowdhury, S.J. Freeman, C.J. Lister, M.P. Carpenter, R.G. Henry, R.V.F. Janssens, T.L. Khoo, T. Lauritsen, Y. Liang, F. Soramel, and I.G. Bearden, *Phys. Rev. Lett.* **72**, 1164 (1994).
- [45] B. Crowell, P. Chowdhury, D.J. Blumenthal, S.J. Freeman, C.J. Lister, M.P. Carpenter, R.G. Henry, R.V.F. Janssens, T.L. Khoo, T. Lauritsen, Y. Liang, F. Soramel, and I.G. Bearden, *Phys. Rev.* **C53**, 1173 (1996).
- [46] P.M. Walker, D.M. Cullen, C.S. Purry, D.E. Appelbe, A.P. Byrne, G.D. Dracoulis, T. Kibédi, F.G. Kondev, I.Y. Lee, A.O. Macchiavelli, A.T. Reed, P.H. Regan, and F. Xu, *Phys. Lett.* **B408**, 42 (1997); P.M. Walker, *Acta Phys. Polonica* **B36**, 1055 (2005).

- [47] N.L. Gjørup, M.A. Bently, B. Fabricius, A. Holm, J.F. Sharpey-Schafer, G. Sletten, and P.M. Walker, *Z. Phys.* **A337**, 353 (1994).
- [48] T. Venkova, T. Morek, G.V. Marti, H. Schnare, A. Krammer-Flecken, W. Gast, A. Georgiev, G. Hebbinghaus, R.M. Lieder, G. Sletten, K.M. Spohr, K.H. Maier, and W. Urban, *Z. Phys.* **A344**, 417 (1993).
- [49] P.M. Walker, *Hyperfine Interact.* **143**, 143 (2002).
- [50] G.D. Dracoulis, S.M. Mullins, A.P. Byrne, F.G. Kondev, T. Kibédi, S. Bayer, G.J. Lane, T.R. McGoram, and P.M. Davidson, *Phys. Rev.* **C58**, 1444 (1998).
- [51] F.G. Kondev, M.A. Riley, D.J. Hartley, R.W. Laird, T.B. Brown, M. Lively, K.W. Kemper, J. Pfohl, S.L. Tabor, and R.K. Sheline, *Phys. Rev.* **C59**, R575 (1999).
- [52] T.R. McGoram, G.D. Dracoulis, T. Kibédi, A.P. Byrne, R.A. Bark, A.M. Baxter, and S.M. Mullins, *Phys. Rev.* **C62**, 031303(R) (2000).
- [53] F.G. Kondev, G.D. Dracoulis, A.P. Byrne, T. Kibédi, S. Bayer, and G.J. Lane, *Phys. Rev.* **C54**, R459 (1996).

FIG. 1: Partial level scheme (part 1 of 2) of ^{180}Re as deduced in the current work.



FIG. 2: Partial level scheme (part 2 of 2) of ^{180}Re as deduced in the current work.

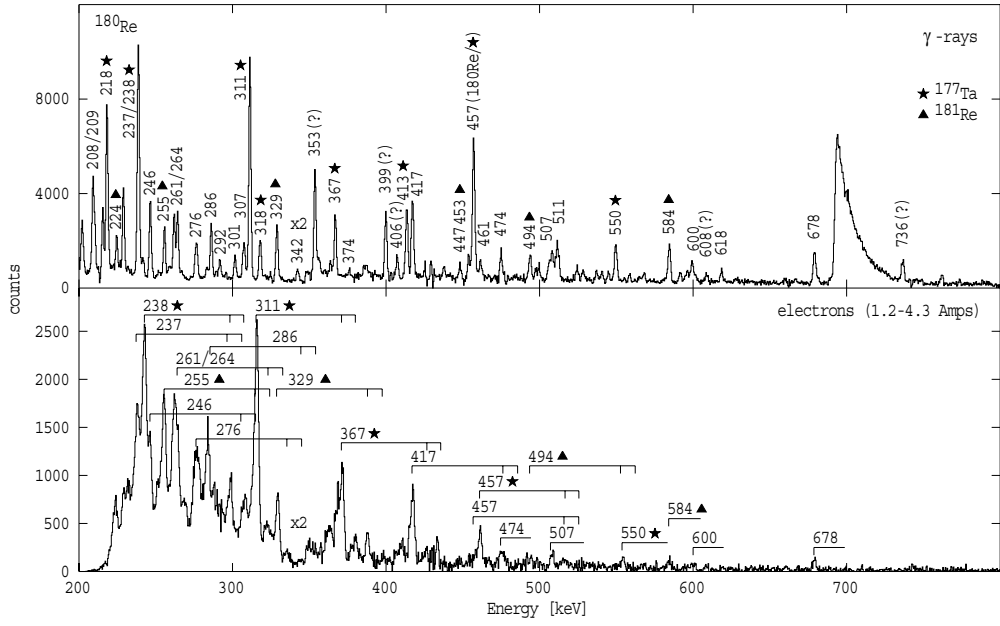


FIG. 3: Spectra for γ rays (top) and electrons (bottom) from the wide sweep of the magnetic field. The electron spectrum has been shifted so that the K-shell transitions in rhenium align with the corresponding γ -ray transitions. Labeled transitions are assigned to ^{180}Re unless indicated otherwise.

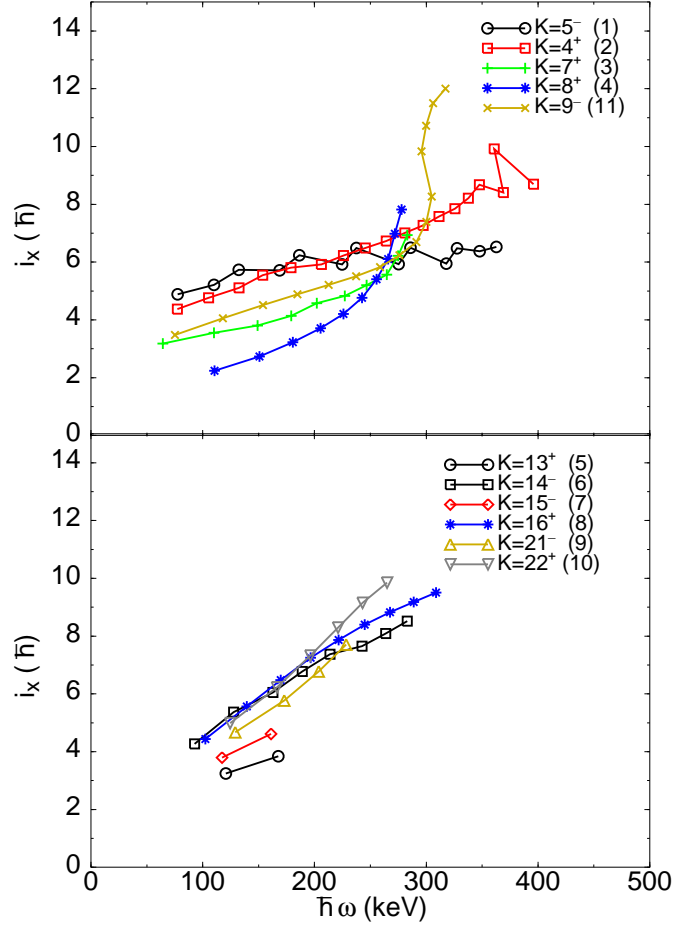


FIG. 4: (Color online) Aligned angular momentum as a function of rotational frequency for the 2-quasiparticle bands (top) and 4- and 6-quasiparticle bands (bottom) in ^{180}Re . The band numbers are given in parentheses. The parameters of the Harris expansion of the reference are $\mathfrak{S}_0=24.1 \text{ MeV}^{-1}\hbar^2$ and $\mathfrak{S}_2=91.1 \text{ MeV}^{-3}\hbar^4$.

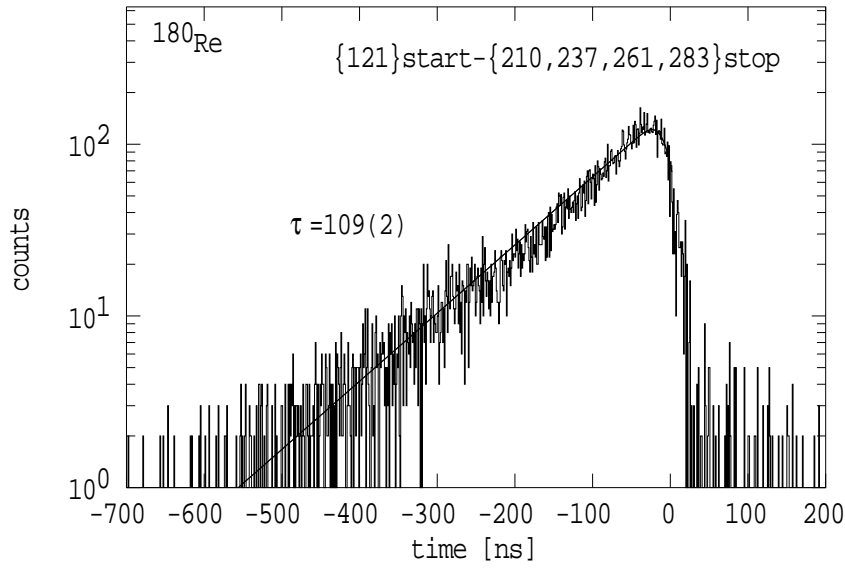


FIG. 5: Summed time-difference spectrum gated across the 284 keV level in ^{180}Re . The mean-life of the isomer is 109 ± 2 ns.

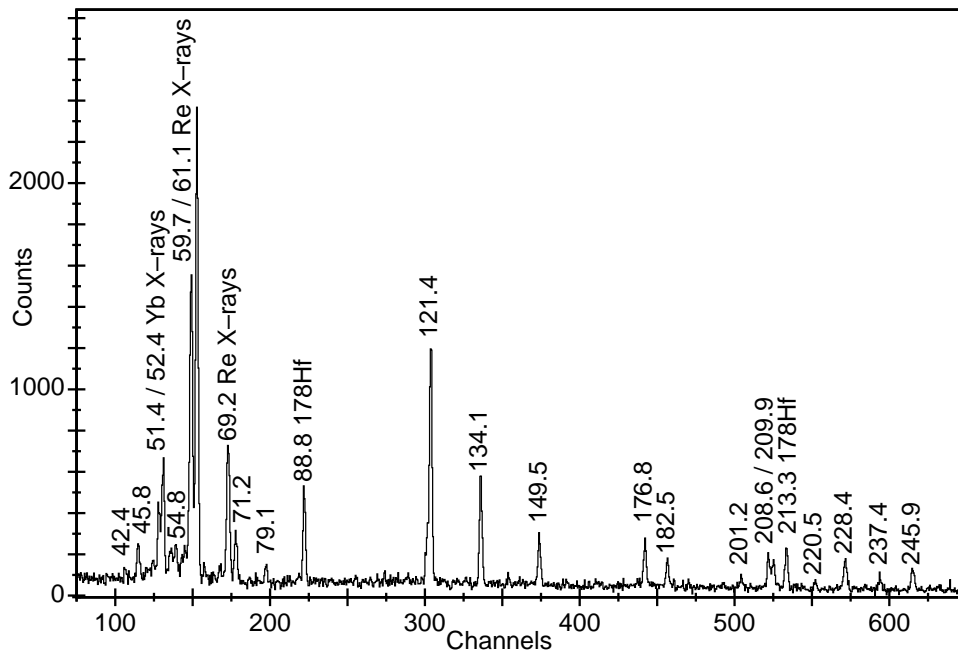


FIG. 6: Coincidence spectrum gated on the 92 keV transition of band 3 in the HPGe detectors to display the 46 keV transition in the LEPS detectors.

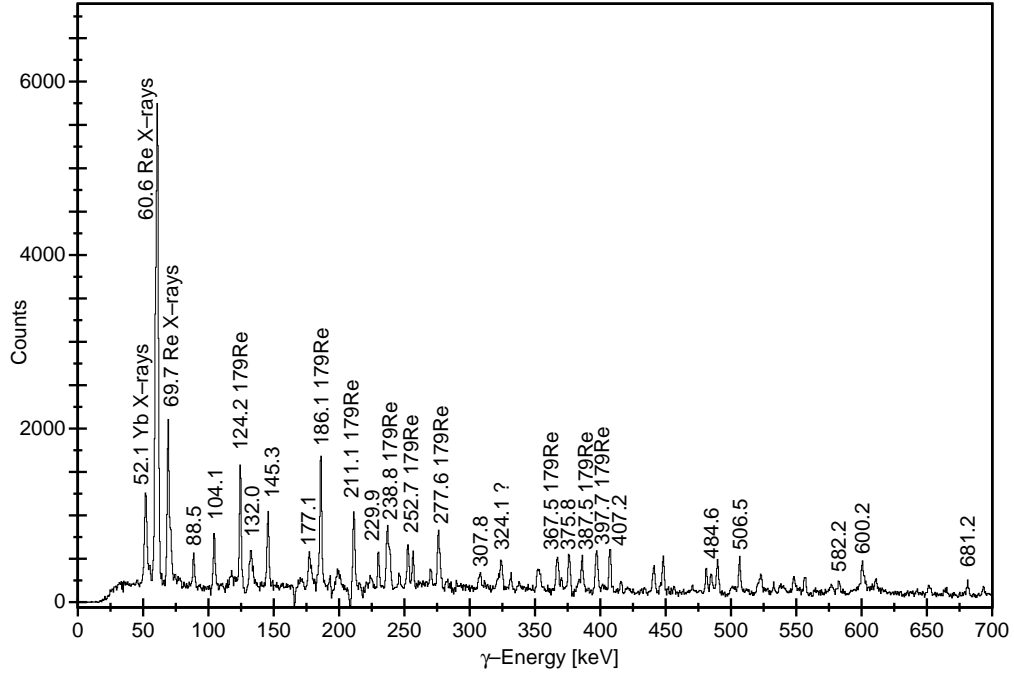


FIG. 7: In-beam γ - γ coincidence spectrum gated on the 156 keV transition to illustrate transitions in band 1, and the 132 keV transition.

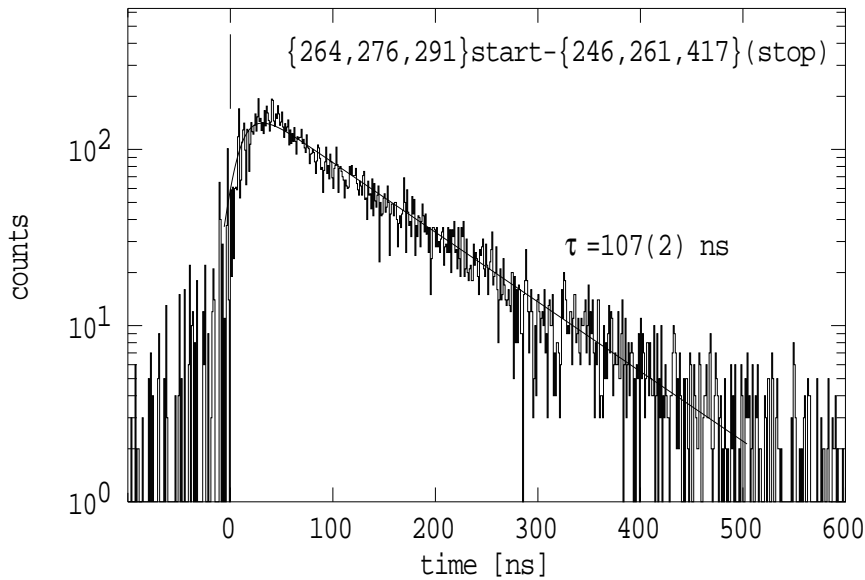


FIG. 8: Summed time-difference spectrum gated across the 1566 keV level in ^{180}Re . The mean-life of the isomer is 107 ± 2 ns, and a feeding component of 7 ± 1 ns is required for the fit (see text).

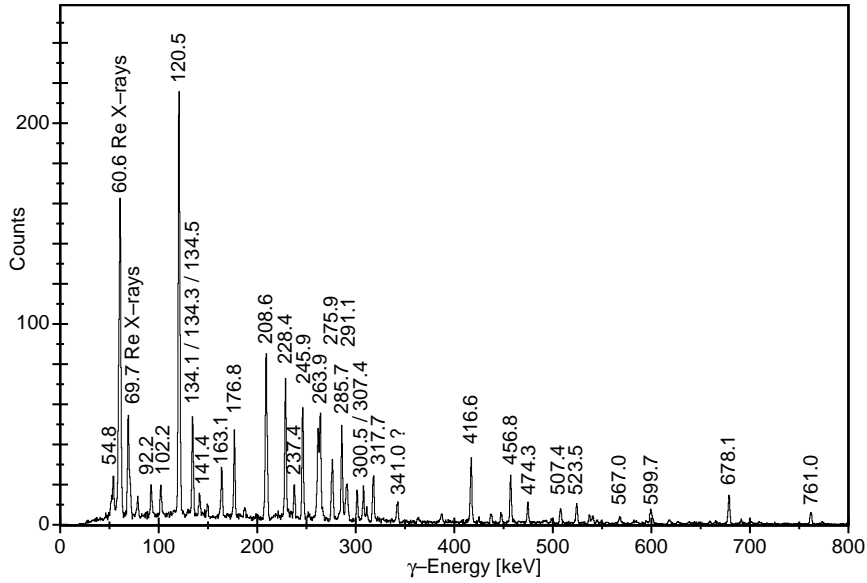


FIG. 9: Coincidence spectrum taken in between beam pulses and gated at 134 keV, showing the 54.8 and 456.8 keV transitions. Note the complexity due to the multiplet of transitions close to 134 keV.

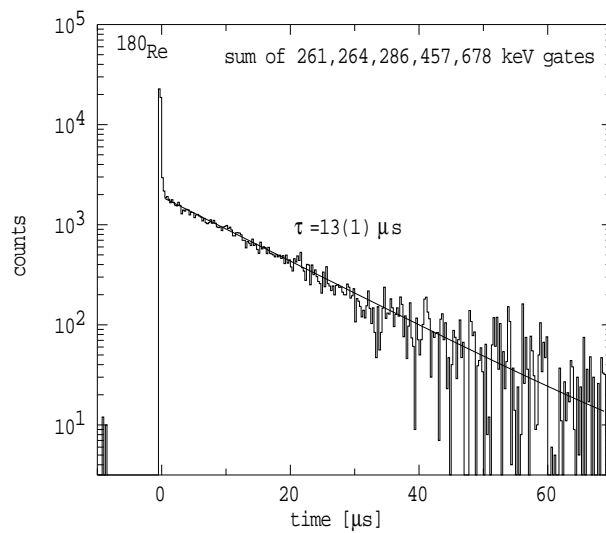


FIG. 10: Summed time spectrum for transitions fed through the 3471.3 keV level in ^{180}Re . Most of the in-beam events have been vetoed in hardware, but a small component remains.

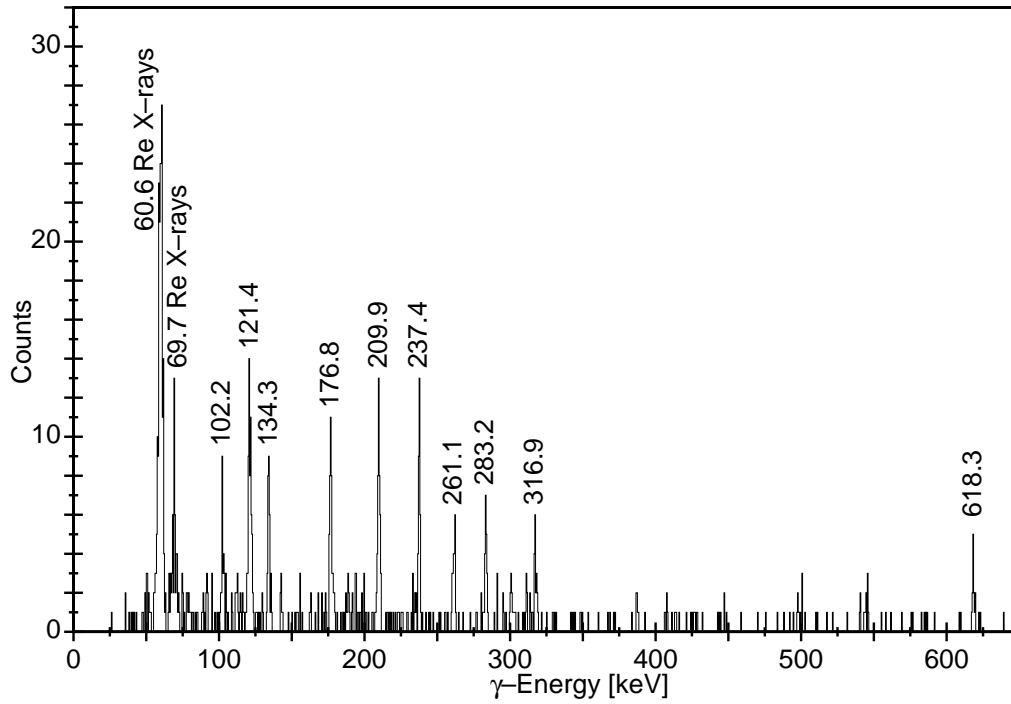


FIG. 11: Out-of-beam γ - γ coincidence spectrum gated by the 1164 keV transition.

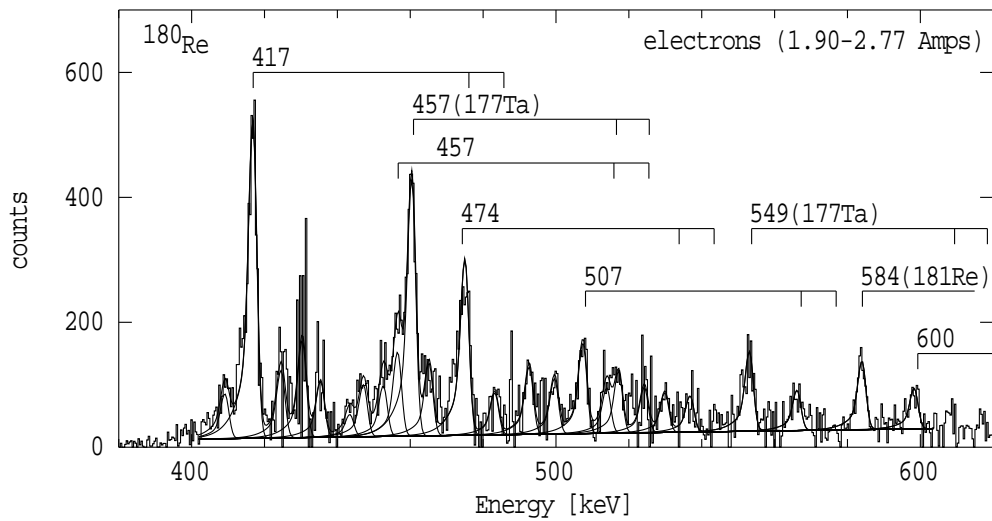


FIG. 12: The electron spectrum for the narrow-sweep magnetic-field measurement showing fits of the 457 keV line in both ^{180}Re and ^{177}Ta .

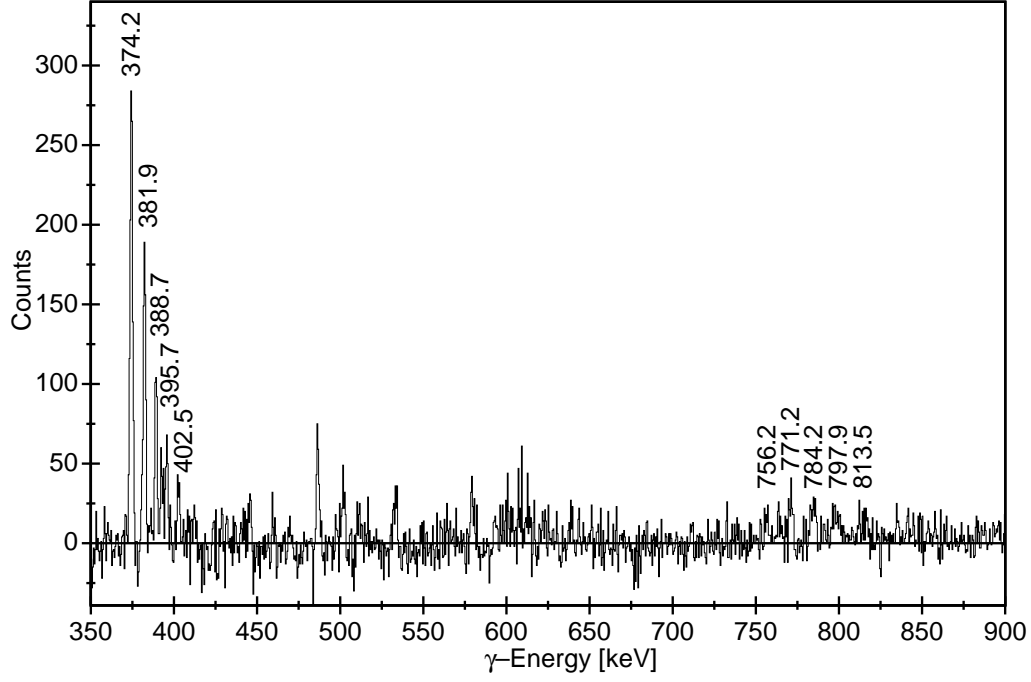


FIG. 13: Coincidence spectrum gated on the 424 keV transition. The labeled peaks are assigned to band 10, $K^\pi=(22^+)$.

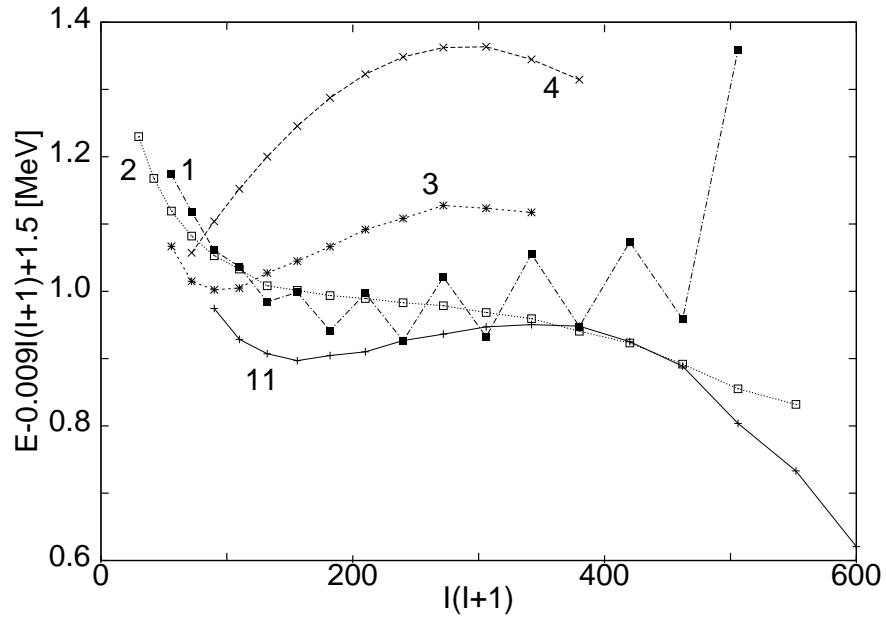


FIG. 14: Energy versus spin diagram of the 2-quasiparticle bands in ^{180}Re . An arbitrary rigid-rotor reference is subtracted from the excitation energies. The following band numbers (and K^π values) are included: 1 (5^-), 2 (4^+), 3 (7^+), 4 (8^+), and 11 (9^-).

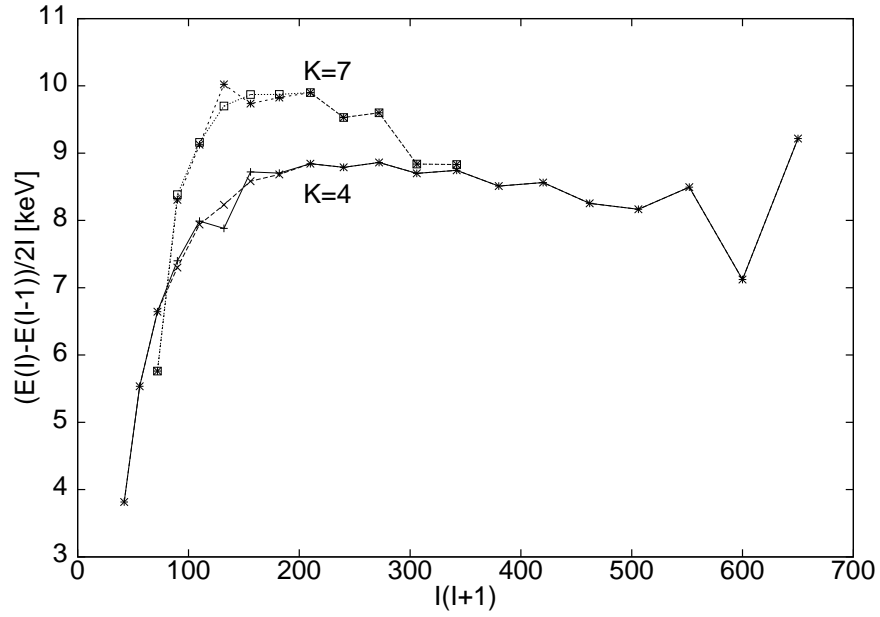


FIG. 15: A plot of $\Delta E/2I$ versus $I(I+1)$ for band 2 ($K=4$) and band 3 ($K=7$). The bands cross at $I=11$. The perturbed (experimental) trajectories in the crossing region can be smoothed by using an interaction matrix element of 7.3 keV to estimate the unperturbed trajectories.

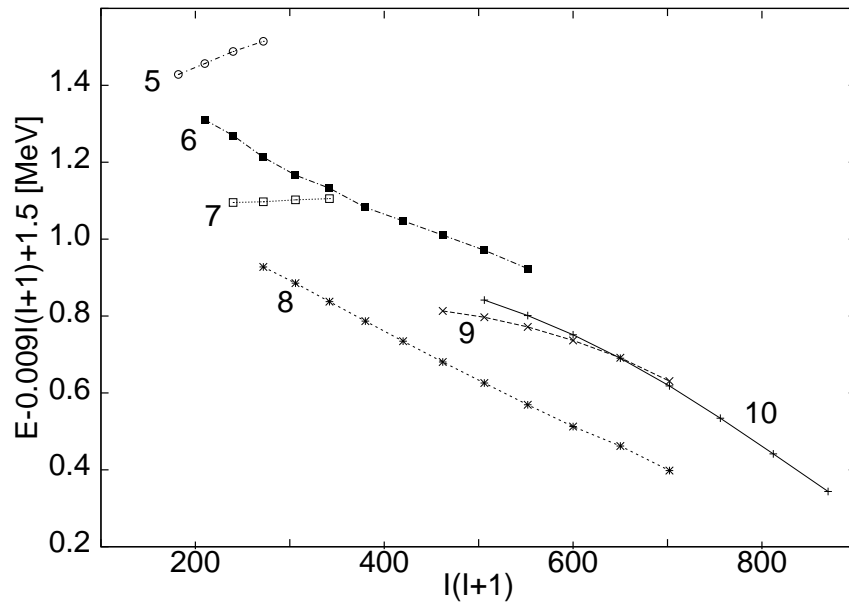


FIG. 16: Energy vs. spin diagram of the 4-, 6-quasiparticle bands in ^{180}Re . An arbitrary rigid-rotor reference is subtracted from the excitation energies. The following band numbers (and K^π values) are included: 5 (13^+), 6 (14^-), 7 (15^-), 8 (16^+), 9 (21^-), and 10 (22^+).

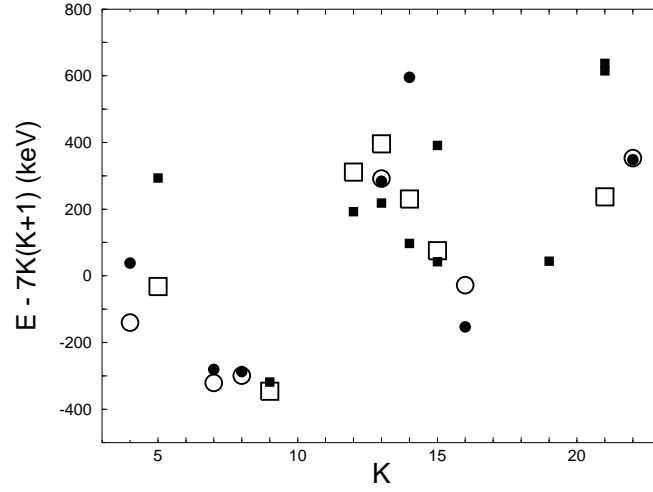


FIG. 17: Comparison, as a function of bandhead spin, between calculated and experimental multi-quasiparticle energies, with a rotor reference subtracted. Open (filled) symbols represent experimental (calculated) states, and circles (squares) represent positive (negative) parity. For each experimental state, the configuration assignment (see text) corresponds to the lowest calculated state of the same spin and parity. Some additional calculated states are shown for comparison.

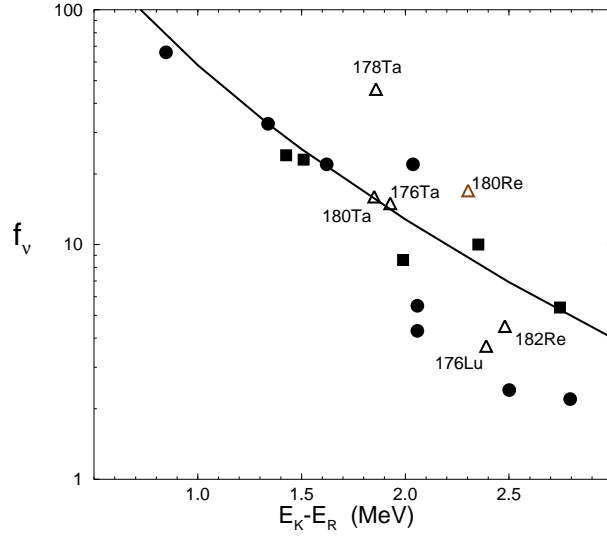


FIG. 18: Variation of reduced hindrance with energy relative to a rigid rotor, for even-even nuclei (filled circles: 4-quasiparticle isomers), odd-mass nuclei (filled squares: 5-quasiparticle isomers) and odd-odd nuclei (open triangles: 4-quasiparticle isomers) adapted from refs [2, 49]. For the odd-mass nuclei, a pairing energy of 0.9 MeV has been added, while 1.8 MeV has been added for odd-odd nuclei. The data are for E2 and E3 decays with $\Delta K \geq 5$. The full line represents the predicted level-density dependence [46].

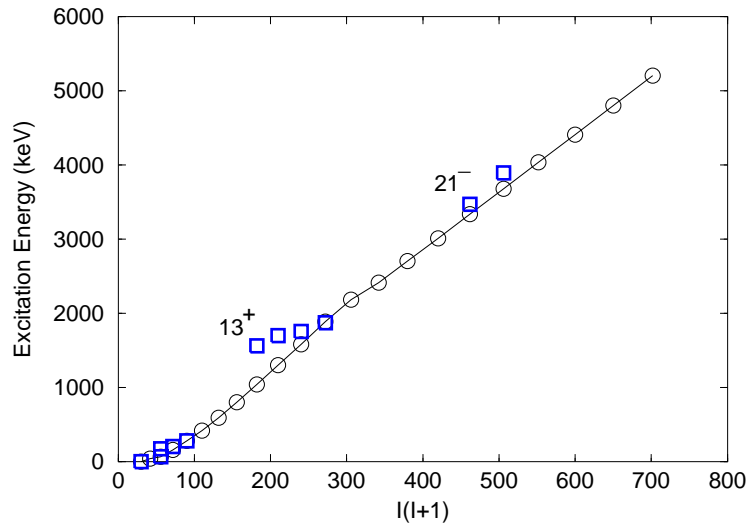


FIG. 19: (Color online) Excitation energy plotted against $I(I+1)$ for the yrast line and intrinsic states in ^{180}Re . Squares denote bandheads. The 4- and 6-quasiparticle isomers are indicated by their K^π values.